https://doi.org/10.5194/hess-2021-426
Preprint. Discussion started: 8 September 2021

Hydrology and Earth System Sciences
Discussions

It rains and then? Numerical challenges with the 1D Richards equation in kilometer-resolution land surface modelling

Daniel Regenass[1,2], Linda Schlemmer[3], Elena Jahr[1], and Christoph Schär[1]

[1]Institute for Atmospheric and Climate Science, ETH Zurich, Zurich, Switzerland
[2]now at Federal Office for Meteorology and Climatology, MeteoSwiss, Zurich Airport, Switzerland
[3]Deutscher Wetterdienst DWD, Offenbach, Germany

Correspondence: Daniel Regenass (daniel.regenass@meteoswiss.ch)

Abstract.

Over the last decade kilometer-scale weather predictions and climate projections have become established. Thereby both the representation of atmospheric processes, as well as land-surface processes need adaptions to the higher-resolution. Soil moisture is a critical variable for determining the exchange of water and energy between the atmosphere and the land surface on hourly to seasonal time scales, and a poor representation of soil processes will eventually feed back on the simulation quality of the atmosphere. Especially the partitioning between infiltration and surface runoff will feed back on the hydrological cycle. Several aspects of the coupled system are affected by a shift to kilometer-scale, convection-permitting models. First of all, the precipitation-intensity distribution changes to more intense events. Second, the time-step of the numerical integration becomes smaller. The aim of this study is to investigate the numerical convergence of the one-dimensional Richards Equation with respect to the soil hydraulic model, vertical layer thickness and time-step during the infiltration process. Both regular and non-regular (unequally spaced) grids typical in land surface modelling are considered, using a conventional semi-implicit vertical discretization. For regular grids, results from a highly idealized experiment on the infiltration process show poor numerical convergence for layer thicknesses larger than approximately $5\,\mathrm{cm}$ and for time steps greater than $40\,\mathrm{s}$, irrespective of the soil hydraulic model. The velocity of the wetting front decreases systematically with increasing time step and decreasing vertical resolution. For non-regular grids, a new discretization based on a coordinate transform is introduced. In contrast to simpler vertical discretizations, it is able to represent the solution second-order accurate. The results for non-regular grids are qualitatively similar, as a fast increase in layer thickness with depth is equivalent to a lower vertical resolution. It is argued that the sharp gradients in soil moisture around the propagating wetting front must be resolved properly in order to achieve an acceptable numerical convergence of the Richards Equation. Furthermore, it is shown that the observed poor numerical convergence translates directly into a poor convergence of infiltration-runoff partitioning for precipitation time series characteristic of weather and climate models. As a consequence, soil simulations with low resolution in space and time may produce almost twice the amount of surface runoff within 24 hours than their high-resolution counterparts. Our analysis indicates that the problem is particularly pronounced for kilometer-resolution models.

https://doi.org/10.5194/hess-2021-426
Preprint. Discussion started: 8 September 2021


Hydrology and Earth System Sciences
Discussions

1 Introduction

Kilometer-scale numerical weather prediction (NWP) and climate models have approached operational use on continental to global scales (Prein et al., 2015; Fuhrer et al., 2018; Leutwyler et al., 2017; Stevens et al., 2019; Schär et al., 2020; Wedi et al., 2020). This marks a major breakthrough in atmospheric modelling, as a large part of vertical energy redistribution can be resolved explicitly and it is reasonable to assume that global kilometer-scale modelling could fundamentally enhance our understanding of the climate system (Palmer, 2014). Numerous publications point out the improved representation of precipitation over land in convection resolving models (CRM hereafter) (e.g Ban et al., 2014; Leutwyler et al., 2017; Pichelli et al., 2021; Vergara-Temprado et al., 2021), in particular the improved representation of the diurnal cycle and rainfall intensities – a long-standing issue in global convection-parameterized NWP and climate models (CPM hereafter) (Stephens et al., 2010). On the one hand, the extensive computational challenges of continental and global convection resolving modelling are evident (Fuhrer et al., 2014; Schär et al., 2020). On the other hand, it is to be expected that higher resolution setups exhibit higher velocities, mass and energy fluxes throughout the whole modelling system, simply as a consequence of reduced spatio-temporal averaging. While this yields exciting possibilities for the investigation of extreme events in a changing climate (Vergara-Temprado et al., 2021, e.g.), it challenges established approaches in numerics and subgridscale parameterizations inherited from CPMs (Yano et al., 2018) – such as the land surface model.

The recent advances in atmospheric modelling are complemented by similar tendencies in global land surface modelling. Wood et al. (2011) view the development of global, comprehensive land surface simulations on the order of 1 km as a "grand challenge" for the hydrologic community. Indeed, recent sub-continental to continental scale three dimensional land surface simulations yield realistic features of the terrestrial water cycle (Maxwell et al., 2015; Mastrotheodoros et al., 2020). However, as is the case for atmospheric science (Yano et al., 2018), there is a fundamental lack of scientific understanding of subgrid-scale processes that ought to be parameterized even on the spatial scales envisaged by Wood et al. (2011) in their grand challenge paper, as has also been pointed out by Beven and Cloke (2012).

In contrast to models of the atmospheric dynamics, land-surface models (LSMs) often do not have a closed system of governing equations, and advances in process understanding are often translated into heuristic implementations. This may deem it impossible for the individual modeler to have an overview on the full LSM and it leads to a large amount of free parameter which are not well constrained by theory (Fisher and Koven, 2020). Moreover, we argue here that it may also lead to a not fully transparent coupling of individual subprocesses within the LSM and with the atmosphere. In addition, numerical aspects of LSMs are receiving much less attention and scrutiny than in atmospheric models, presumably because of the important role of semi-empirical concepts.

Indeed, this study is partially motivated by challenges the authors faced while trying to test and calibrate a new groundwater model for the TERRA ML LSM (Heise et al., 2003) presented by Schlemmer et al. (2018). When comparing a CPM to a CRM

https://doi.org/10.5194/hess-2021-426
Preprint. Discussion started: 8 September 2021


Hydrology and Earth System Sciences
Discussions

simulation with the COSMO model (Baldauf et al., 2011), Ban et al. (2014) found that soil moisture is generally lower during summer in the CRM simulation. Of course there might be multiple factors involved, but Keller (2016, pp. 59 - 67) provide reasonable arguments that the underlying reason is the shift from more frequent, less intense to less frequent, more intense precipitation events in CRM simulations. The precipitation intensities in CRM simulations exceed the maximum infiltration capacity more often. This leads to more surface runoff and less infiltration of water into the soil. The problem can be alleviated by introducing a depth-dependent profile of saturated hydraulic conductivity as has been suggested by Decharme et al. (2006). Even after introducing the Decharme et al. (2006) formulation for saturated hydraulic conductivity, there are marked differences in water partitioning at the surface for CRM and CPM simulations. This is illustrated in Fig. 1, which shows precipitation and surface runoff sums as obtained from simulations carried out with the COSMO model (Baldauf et al., 2011) following the same setup as used by Zeman et al. (2021) for May 29 2018, a day characterized by convective activity across the entire European continent. Overall, the CRM simulation exhibits higher precipitation sums than the CPM simulation and, more intricate, overall higher amounts of surface runoff. Just by comparing differences in precipitation to differences in surface runoff (Fig. 1, bottom row), it becomes clear that the relation between the two is not trivial. Differences in surface runoff are more patchy, likely an indication for the important role high-intensity precipitation events and surface heterogeneity play for the observed differences in partitioning of water at the surface. The difference between the two quantities in turn represent the water that infiltrates into the soil, which may influence the storage and thus long-term memory of the soil.

The understanding of relevant physical processes and relevant model parameters is further obscured, as in some LSMs, numerical and physical approximations of the real-world problem are not fully separated. On the physical side, the challenge lies in the accurate estimation of saturated hydraulic conductivity – or even broader, finding a suitable approach to the infiltration problem on the kilometer-scale. This is then followed by the numerical representation of the governing equation for water transport in the soil matrix (in this case the Richards (1931) equation). This has become evident as the authors observed time step and resolution dependencies in the generation of surface runoff in standalone applications of TERRA ML.

As is the case for TERRA ML, most 2nd and 3rd generation LSMs describe water transport in the soil matrix by some form of the one-dimensional Richards (1931) equation (Pitman, 2003). This 'backbone' of the hydrology section has not changed dramatically in current state-of-the art LSMs (Balsamo et al., 2009; Niu et al., 2011; Ducharne, 2016; Lawrence et al., 2019; Reick et al., 2021). Extensions to LSM hydrology have primarily focused on groundwater parameterizations (Niu et al., 2007; Schlemmer et al., 2018) and infiltration-runoff partitioning (Liang et al., 1994; Niu et al., 2005). Recently,some effort is invested into incorporating new pedotransfer functions into LSMs and it is clear that the choice of pedotransfer functions affects the model properties substantially (Weihermüller et al., 2021). Modern methods to estimate pedotransfer functions (Schaap et al., 2001; Saxton and Rawls, 2006; Van Looy et al., 2017) have a continuous dependency on soil texture instead of being fixed for discrete soil classes and account for organic matter in the soil. Such pedotransfer functions facilitate the use of high resolution maps of soil properties (most notably SoilGrids250m, Hengl et al., 2017).

In contrast to the efforts in adding more realism to soil physical aspects, numerical aspects of the Richards equation have

https://doi.org/10.5194/hess-2021-426
Preprint. Discussion started: 8 September 2021

Hydrology and Earth System Sciences
Discussions

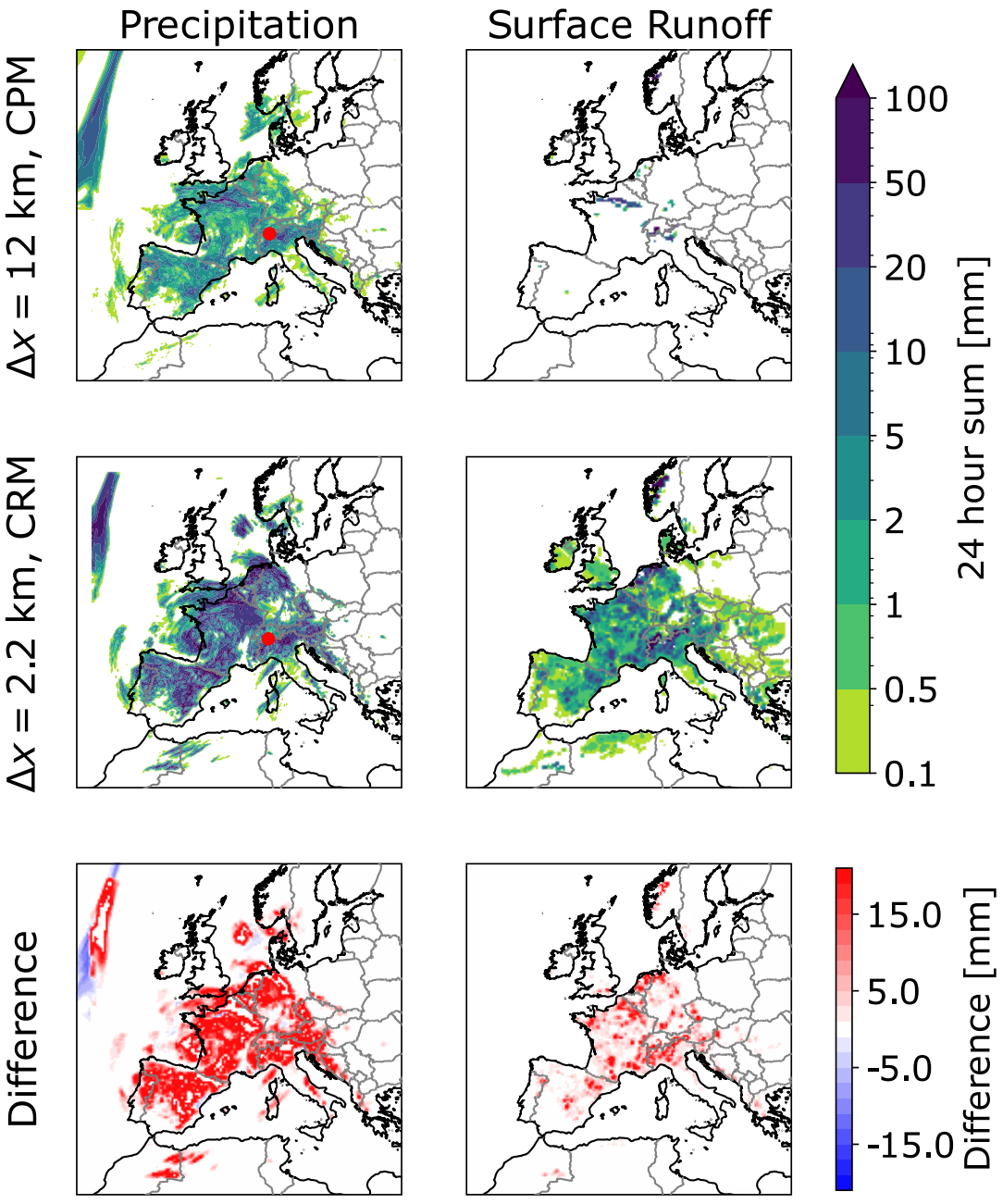

Figure 1. 24-hour precipitation and surface runoff sums for May 29, 2018 as obtained from two simulations using the setup of Zeman et al. (2021), using parameterized (top) and explicit (middle) convection. The bottom row shows differences CRM–CPM in precipitation and surface runoff on the 12 km grid. The red points in the precipitation plot mark the center of two convective cells near the village of Baceno (2.2 km simulation) and Pizzo Tambo (12 km simulation).

https://doi.org/10.5194/hess-2021-426
Preprint. Discussion started: 8 September 2021


Hydrology and Earth System Sciences
Discussions

received much less attention. Nevertheless, there seems to be some awareness of numerical issues in the LSM community. Already quite early after the implementation of Richards equation into LSMs, Lee and Abriola (1999) pointed out that vertically integrated solutions of the Richards equation – as used by many LSMs at that time and still today – tend to overpredict soil moisture in the uppermost layers and underpredict discharge to the aquifer. Campoy et al. (2013) drastically increased the number of vertical layers to conduct experiments concerning the choice of the bottom boundary condition in ORCHIDEE. Zeng and Decker (2009) tried to reduce truncation errors of the spatial discretization by subtracting the equilibrium soil moisture from the equation. An approach that was later discarded by Lawrence et al. (2019) due to problems pointed out by De Rooij (2010). Lawrence et al. (2019) recently introduced an adaptive time-stepping procedure developed by Kavetski et al. (2001) in order to improve numerical stability of solutions to the Richards equation. Mueller-Quintino et al. (2016) compared three LSMs and found spurious oscillations at low vertical resolutions. However, there seems to be a lack of systematic assessment concerning the magnitude of numerical errors introduced by solving the Richards equation with standard approaches and setups.

In order to elucidate the problem of numerical errors, this paper addresses the following research questions: Do numerical representations of the solution to the 1D Richards Equation as used in land surface models converge? How good is the convergence? What are the implications for the infiltration process? How do numerical errors interact with rainfall intensities as obtained from CPM and CRM simulations, respectively? What are the implications for kilometer-scale weather and climate modeling?

The remainder of this paper is organized as follows: The model and its numerical representation are introduced in section 2. The convergence experiments are described in section 3 and the corresponding results are presented in section 4. Finally, some final thoughts and our conclusions are formulated in section 5.

2 Model

In the first part of this section, the derivation of the one-dimensional Richards Equation is briefly revisited and two different soil hydraulic models are discussed. In the second part, the numerical implementation is presented and a novel coordinate transform for the one-dimensional Richards Equation on non-equidistant grids is introduced. The soil model described in this section is implemented in Python.

2.1 The System Under Consideration

In the following sections, a model of one-dimensional water transport in a homogeneous, porous medium will be introduced. Let us first take a step back in order to get a feeling for the system described by the one-dimensional Richards equation. A related physical experiment is shown in Fig. 2 (although the transport here is not strictly one dimensional, but sufficiently close). There are three main observations to be highlighted: First, even in a setup as homogeneous as depicted in Fig. 2 preferential flow paths seem to form, where water transport happens faster. On the order of LSM grid cells or tiles, the inhomogeneities are substantially larger and should be accounted for, but this is beyond the scope of this paper. Second – and this is important for the numerical solution of Richards equation – there is a sharp gradient in soil moisture from the wet to the dry zone, the so-called

https://doi.org/10.5194/hess-2021-426
Preprint. Discussion started: 8 September 2021

Figure 2. Do-it-yourself infiltration experiment with a sand column. Water is poured at the top of the column, and the panels show the infiltration after five minutes (left) and one hour (right). Note the sharp gradient in the transition from wet to dry sand - the so-called wetting front. The propagation velocity of the wetting front determines the infiltration rate and hence the amount of ponding water on the surface.

wetting front, which is a characteristic feature of water propagation in porous media. This sharp gradient must be mirrored in some way in the soil hydraulic model and ideally be captured by the spatial and temporal discretization. Finally, notice the water ponding on top of the soil column which almost completely vanishes after one hour of infiltration. The propagation of the wetting front determines the amount of water that may infiltrate the soil.

2.2 Mathematical Formulation

2.2.1 Governing Equation

Let us consider an arbitrary element of soil with volumetric soil moisture θ in a Cartesian coordinate system. Mass conservation reads

$$\frac{\partial \theta}{\partial t} = -\nabla \cdot \mathbf{F} - E \,, \tag{1}$$

where $\mathbf{F}$ is the volumetric soil water flux in $\mathrm{m/s}$ and E is a sink term due to local evapotranspiration. Infiltration is given as a boundary condition for the vertical flux at the surface, i.e. $\mathrm{F_z(z = 0) = I}$. Let us now assume that the flux F follows Darcy's law

$$\mathbf{F} = -K \nabla h \,, \tag{2}$$

with hydraulic conductivity K and hydraulic head $h = \psi + z_t - z$. The hydraulic head in unsaturated soils is the sum of suction head ψ and gravitational head $z_t - z$, where z_t is the topographic height and z is the depth beneath the local surface. We

https://doi.org/10.5194/hess-2021-426
Preprint. Discussion started: 8 September 2021


Hydrology and Earth System Sciences
Discussions

introduce the horizontal Nabla $\nabla_h = (\partial/\partial x,\ \partial/\partial y)$ and separate lateral and vertical flow (thereby moving to a downward pointing vertical coordinate z) to obtain

$$\frac{\partial\theta}{\partial t} = -\frac{\partial}{\partial z}\left(-K\frac{\partial h}{\partial z} + K\right) + \nabla_h \cdot K\nabla_h(\psi + z_t - z) - E\ . \tag{3}$$

Due to computational constraints, lateral flow is often neglected or parameterized. Here, lateral flow is treated as a source/sink term $Q = -\nabla_h \cdot K\nabla_h(\psi + z_t - z)$ and we will discuss its parameterization in section 2.2.3. Using this simplification, applying the chain rule and introducing hydraulic diffusivity $D(\theta) = K(\theta)\partial h/\partial\theta$, we can rewrite (3) as (Hillel, 2012)

$$\frac{\partial\theta}{\partial t} = -\frac{\partial}{\partial z}\left(-D(\theta)\frac{\partial\theta}{\partial z} + K(\theta)\right) - E - Q\ . \tag{4}$$

This is the one-dimensional saturation-based form of Richards Equation which shall be used subsequently. As a number of LSMs in operational NWP and climate models use the saturation form of the Richards equation (Heise et al., 2003; Balsamo et al., 2009; Ducharne, 2016; Reick et al., 2021, mainly at European weather services and research institutions, see), we will base our analysis on it. In land surface modelling, evapotranspiration is usually estimated in a different part of the model which is beyond the scope of this paper. Therefore, we set $E = 0$ for all further derivations and experiments in this study. Still missing are expressions for K, D and Q, which we will introduce in the following subsections.

2.2.2 Soil Hydraulic Model K, D

Following Shao and Irannejad (1999), the functions K and D will be referred to as the soil hydraulic model. Here, two different soil hydraulic models are tested. On the one hand, the Rijtema (1969) model (RT model hereafter) with exponential dependencies on saturation which is used in TERRA ML (Heise et al., 2003), and on the other hand the Mualem (1976) - Van Genuchten (1980) model (MVG model hereafter) with stronger dependencies on soil moisture close to saturation and air dry point, which is preferred by many soil physicists (Shao and Irannejad, 1999). Both models require a number of parameters which depend on soil texture. In this study, parameters are chosen for a loam soil. All parameters and the hydraulic functions are summarized in Table 1. There is one important detail in the MVG model which requires some consideration: The hydraulic diffusivity D diverges as the relative moisture θ_f approaches saturation (see A and Van Genuchten (1980)). In practice, D has to be limited to finite values. In ORCHIDEE, this is achieved by piecewise discretization of the function $D(\theta)$ with respect to θ. The value of the last interval (with the relative moisture content $\theta_f = 1$ as upper bound) is then set to a fraction of the second but last interval (Ducharne, 2016). In HTESSEL (Balsamo et al., 2009) and JSBACH (Reick et al., 2021), D is modeled after the equation given by Clapp and Hornberger (1978), while K is still given by the MVG model. This is somewhat contradictory to the idea of Van Genuchten (1980), where the model is presented as a closed system of equations. Here, we limit the value of D to the tenfold value of saturated hydraulic conductivity. All of these approaches are rather heuristic and the underlying reason is likely that finite values of D at saturation are not compatible with fundamental physical properties of this quantity (see A). The seemingly arbitrary choice for a maximum value of D is of some importance to the convergence of Richards Equation, as a higher value of D near saturation weakens the strong gradients around the wetting front and therefore improves numerical convergence (see B).

https://doi.org/10.5194/hess-2021-426
Preprint. Discussion started: 8 September 2021

Hydrology and Earth System Sciences
Discussions
Open Access
EGU

Symbol/ Unit	Parameter/ Variable	RT	MVG
$\eta\,[\mathrm{m}^3/\mathrm{m}^3]$	Pore Volume	0.455	0.43
$\alpha_{dp}\,[\mathrm{m}^3/\mathrm{m}^3]$	Air Dry Point	0.035	0.078
$K_0\,[\mathrm{m/s}]$	Saturated Hydraulic Conductivity	$5.34 \cdot 10^{-6}$	$2.89 \cdot 10^{-6}$
$K_1\,[-]$	RT Conductivity Coefficient	-19.88	-
$D_0\,[\mathrm{m}^2/\mathrm{s}]$	Saturated Hydraulic Diffusivity	$357 \cdot 10^{-8}$	-
$D_1\,[-]$	RT Diffusivity Coefficient	-7.44	-
$\alpha\,[\mathrm{m}^{-1}]$	MVG Parameter	-	3.6
$m\,[-]$	MVG Parameter	-	0.359
$\theta_f\,[\mathrm{m}^3/\mathrm{m}^3]$	Relative Moisture Content	-	$\theta_f = (\theta - \alpha_{dp}) / (\eta - \alpha_{dp})$
$K\,[\mathrm{m/s}]$	Hydraulic Conductivity	$K = K_0 \exp\left(K_1 \frac{\eta-\theta}{\eta-\alpha_{dp}}\right)$	$K = K_0 \sqrt{\theta_f} \left(1 - \left(1 - \theta_f^{1/m}\right)^m\right)^2$
$D\,[\mathrm{m}^2/\mathrm{s}]$	Hydraulic Diffusivity	$D = D_0 \exp\left(D_1 \frac{\eta-\theta}{\eta-\alpha_{dp}}\right)$	$D = \frac{(1-m)K(\theta)}{m\alpha} \frac{1}{\theta-\alpha_{dp}} \theta_f^{-1/m} \left(\theta_f^{-1/m} - 1\right)^{-m}$

Table 1. MVG and RT soil hydraulic models. Parameters for a loam soil and hydraulic functions K and D.

Exp	Grid Layout	Number of Vertical Layers	Time Steps (Δt) [s]	Parameterization	Forcing
AR	Regular	200, 100, 50, 40, 25, 20	1, 2, 5, 10, 20, 40, 80, 160, 320	MVG, RT	20 mm/h constant
AG	Telescope	200, 110, 49, 32, 18, 11, 8	1, 2, 5, 10, 20, 40, 80, 160, 320	MVG, RT	20 mm/h constant
B	Telescope	200, 110, 49, 32, 18, 11, 8	20, 90, 180	MVG	Model Rain 2.2 km, 12 km / 20s, 90s

Table 2. Overview on all numerical experiments carried out in this study.

https://doi.org/10.5194/hess-2021-426
Preprint. Discussion started: 8 September 2021


Hydrology and Earth System Sciences
Discussions

2.2.3 Ground Runoff Q

In order to parameterize the effect of topography on ground runoff, Schlemmer et al. (2018) implemented a formulation for ground runoff from the saturated part of the soil which should in principle be independent from the horizontal resolution of the land surface model. They assume runoff divergence (the horizontal contribution to (3)) from the saturated part of the soil column (from bedrock z_B to the upper limit of the water table z_{wt}) to be given by

$$Q = L_g^{-1} \cdot K_0 \cdot S_{\mathrm{ORO}} \,, \tag{5}$$

where S_{ORO} is a slope parameter representing the sub-gridscale gradient of orography and L_g^{-1} is the inverse of the dominant length scale of sub-gridscale heterogeneity. Note that the part $K_0 \cdot S_{\mathrm{ORO}}$ is equivalent to Darcy flow from the saturated zone. In this formulation Q is strictly positive due to the specific formulation of S_{ORO} (see Schlemmer et al. (2018) for details). The rationale of this approach is to include the water table in the soil column and to diagnose the position of the water table and subsequently ground runoff. The water table has to be diagnosed each time step, the procedure takes water from the saturated zone as well as from the layer above into consideration, the details are given in Schlemmer et al. (2018). Note that this parameterization requires a zero-flux boundary condition in order for the water table to build up.

2.2.4 Boundary Conditions

As implied in section 2.2.3, there is no bottom drainage in the Schlemmer et al. (2018) model and therefore the bottom boundary condition is given by

$$K(z = z_B) = 0, \qquad D(z = z_B) = 0\,. \tag{6}$$

The upper boundary condition is given by infiltration I, which is on the one hand given by downward water flux at the surface (precipitation, snow melt, etc.) denoted with P hereafter. On the other hand I is controlled by maximum infiltration I_{MAX} which cannot exceed saturated hydraulic conductivity at the surface $I_{MAX} \leq K_0(z = 0)$ and furthermore it is limited by available pore space at the surface. The former limitation is straightforward to implement, the latter is subject to the numerical implementation. Surface runoff is then given by the difference of downward water flux at the surface and infiltration,

$$Q_S = P - I\,. \tag{7}$$

2.3 Numerical Implementation for Equidistant Grids

As is the case for many land surface models (see e.g. Ducharne, 2016; Lawrence et al., 2019; Heise et al., 2003), Richards Equation is solved on a staggered grid with the fluxes on the layer interfaces (Fig. 3). Here, the layers are chosen to be equidistant, a method for non-equidistant grids will be introduced in section 2.4. In order to capture the sharp gradients in soil moisture around the wetting front, relatively thin layers are required. Therfore, to ensure numerical stability, a semi-implicit time stepping procedure is chosen. The diffusive part of (4) is solved with a simplified backward-implicit time stepping. The

https://doi.org/10.5194/hess-2021-426
Preprint. Discussion started: 8 September 2021

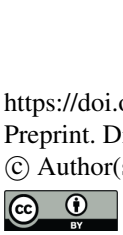

Hydrology and Earth System Sciences
Discussions

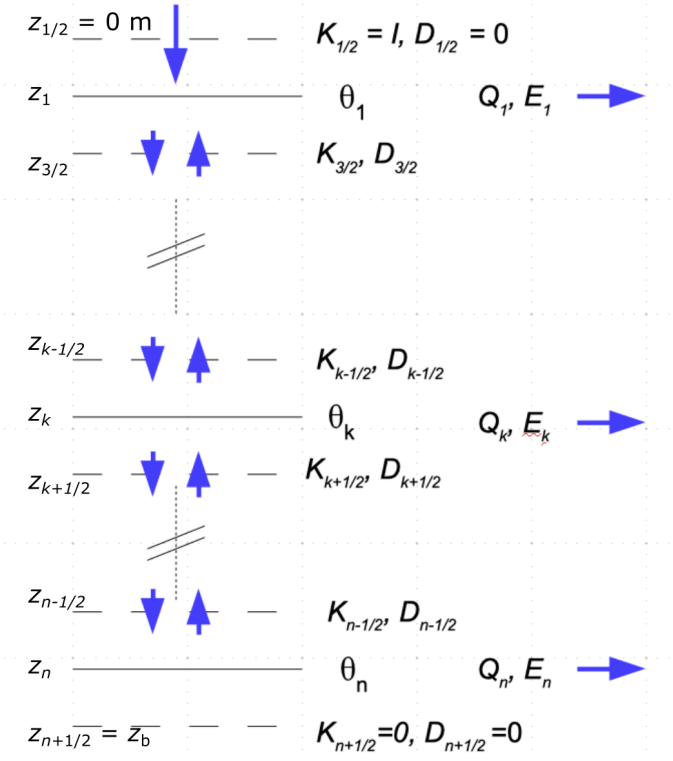

Figure 3. Vertical discretization of the soil column. θ is volumetric soil moisture, K and D are conductive and diffusive fluxes, Q and E are sink terms related to net runoff and evapotranspiration respectively. The indices k are chosen for full levels and the indices $k_{+/-1/2}$ for half-levels (layer interfaces).

simplification hereby is that the functions K and D use the volumetric soil moisture of time level m (instead of $m+1$). Using the presented spatial discretization and the semi-implicit time-stepping, the discretized form of (4) reads

$$\begin{aligned}&\frac{\theta_k^{m+1}-\theta_k^m}{\Delta t} = \\ &\frac{1}{\Delta z}\left(D(\theta_{k+1/2}^m)\frac{\theta_{k+1}^{m+1}-\theta_k^{m+1}}{\Delta z}\right. \\ &\left.-D(\theta_{k-1/2}^m)\frac{\theta_k^{m+1}-\theta_{k-1}^{m+1}}{\Delta z}\right) \\ &-\frac{1}{\Delta z}\left(K_{k+1/2}(\theta_{k+1/2}^m)+K_{k-1/2}(\theta_{k-1/2}^m)\right)-Q_k-E_k\,.\end{aligned} \tag{8}$$

Solving for θ_k^{m+1} on all levels k leads to a tridiagonal linear system of equations which can be solved using standard methods. Note that the explicit part of (8) uses flux corrected quantities for K and Q as introduced by Schlemmer et al. (2018) following the flux-corrected transport (FCT) method after Boris and Book (1973) and Zalesak (1979). This ensures mass conservation even in the fully saturated part of the soil and close to the air dry point. A special case of the flux correction for overfill (see

https://doi.org/10.5194/hess-2021-426
Preprint. Discussion started: 8 September 2021


Hydrology and Earth System Sciences
Discussions

Schlemmer et al., 2018, Eq. (43)) concerns infiltration, which is limited by

$$I^m_{max} = \min\left[I^m_K, \tilde{\tilde{K}}^m_{1/2} + \Delta z_1 \left(\frac{\eta - \theta^m_1}{\Delta t} - \tilde{Q}^m_1\right)\right], \tag{9}$$

where $\tilde{\tilde{K}}^n_{1/2}$ and $\tilde{Q}^n_1$ are (flux corrected) gravitational flux across the bottom of the first layer and ground runoff from the first layer respectively and $I^m_K = \min(P, K_0(z=0))$ is conductivity limited infiltration (see section 2.2.4).

2.4 Coordinate Transformation for Non-Equidistant Grids

In land surface modelling, it is common to choose a grid with thinner layers close to the surface to capture the infiltration more accurately. At the same time the coarser grid at larger depths allows deeper soils without becoming computationally too expensive. While this seems reasonable at first glance, it should be stressed that (8) is second order accurate only if the layers are chosen to be equidistant. For non-equidistant grids, (8) would introduce first-order errors to the solution (Sundqvist and Veronis, 1970). In this section, (8) is transformed to allow for geometric grids while retaining second-order accuracy ('geometric' as the layer thicknesses can be expressed as a geometric series).

2.4.1 Transformed Equation

Let us introduce ζ such that $z = f(\zeta)$, where f is continuously differentiable on the region of interest and the inverse function is continuously differentiable. Using the chain rule, the derivatives in the governing equation (5) can be expanded to yield

$$\frac{\partial\theta}{\partial t} = -\frac{\partial}{\partial\zeta}\left(-D(\theta)\frac{\partial\theta}{\partial\zeta}\frac{\partial\zeta}{\partial z} + K(\theta)\right)\frac{\partial\zeta}{\partial z} - E - Q\,. \tag{10}$$

The transformed equation (10) can not be rearranged into flux form and it would thus be incompatible with the FCT method. To overcome this issue, (10) is multiplied with the inverse of the metric term $J^{-1} = \partial z/\partial\zeta$ to obtain,

$$\frac{\partial\hat{\theta}}{\partial t} = -\frac{\partial}{\partial\zeta}\left(-JD(\theta)\frac{\partial\theta}{\partial\zeta} + K(\theta)\right) - \hat{E} - \hat{Q}\,, \tag{11}$$

where $J = \partial\zeta/\partial z$ is the metric term and the '$\hat{}$' indicates transformed quantities, e.g. $\hat{\theta} = J^{-1}\theta$. For the implementation, it is important to note that θ appears in its transformed and non-transformed state and some care has to be taken to avoid inconsistencies when setting up the linear system of equations.

2.4.2 Suggestion for a Geometric Grid

The aim of the transformation is to put more layers close to the surface and fewer layers in the deep soil, where the time scales are often assumed to be larger and the spatial gradients of soil moisture less sharp. An exponential increase of layer thickness seems to be a reasonable approach and we use

$$\zeta(z) = \ln\left(\frac{b}{\Delta z_1}z + 1\right) \iff z(\zeta) = \frac{\Delta z_1}{b}\left(e^\zeta - 1\right)\,. \tag{12}$$

https://doi.org/10.5194/hess-2021-426
Preprint. Discussion started: 8 September 2021


Hydrology and Earth System Sciences
Discussions
Open Access
EGU

This transformation has two parameters, the dimensionless constant b that controls the increase in thickness from one layer to the next and Δz_1, the thickness of the uppermost layer. Upon requesting $\zeta(\Delta z_1) = \Delta\zeta$ using 12, the equation connecting b and $\Delta\zeta$ can be derived as

$$\Delta\zeta = \ln(1+b) \ . \tag{13}$$

It is then straightforward to show that the layer thickness of layer k is given by

$$\Delta z_k = (1+b)\,\Delta z_{k-1} = (1+b)^{k-1}\,\Delta z_1 \ , \tag{14}$$

and using the summation rule for geometric series, the depth of nth layer interface is located at

$$z_{n+1/2} = \Delta z_1 \frac{(1+b)^n - 1}{b} \ . \tag{15}$$

For the limit $b \to 0$, the regular grid is recovered if $\Delta\zeta$ is chosen according to (13). To complete the transformation rules for this specific transformation, we calculate the metric term at layer k to be

$$\left(\frac{\partial\zeta}{\partial z}\right)_k = \frac{1}{z_k + \frac{\Delta z_1}{b}} \ , \tag{16}$$

and its inverse

$$\left(\frac{\partial z}{\partial\zeta}\right)_k = z_k + \frac{\Delta z_1}{b} = \frac{\Delta z_1}{b} e^{\zeta_k} \ . \tag{17}$$

The metric terms for the layer interfaces may be calculated analogously.

3 Description of the Numerical Experiments

All experiments are carried out with a soil depth of 2 m meaning that the first layer interface (i.e. the surface) is at $z = 0\,\mathrm{m}$ and the last interface is at $z = 2\,\mathrm{m}$. An initially moist environment is chosen with $\theta_{init} = 0.8\eta$. Parameter choices related to the soil hydraulic model are given in Table 1. Evapotranspiration is switched off for all experiments in order to focus solely on infiltration and drainage processes.

3.1 Grid Layouts

Two grid layouts are considered in this study. On the one hand, convergence is investigated for regular grids with the implementation discussed in section 2.3. In this case, the number of grid layers n_z is given by $n_z = z_b/\Delta z$. On the other hand, experiments are carried out with the geometric grid introduced in section 2.4.2 with the necessary adaptions in the solver (section 2.4). For all experiments with the geometric grid, the first layer is fixed to a thickness of $\Delta z_1 = 0.01\,\mathrm{m}$. Suitable combinations of b and n_z were found in the following way: Starting from fixed values for the stretch factor $b = 0.01, 0.05, 0.1, 0.25, 0.5, 1$, the number of levels was then fixed by trial and error such that the total depth was as close to 2 m as possible. Eq. (15) is solved for b with $z_{n+1/2} = z_b$ using Newton's method. The resulting grid layouts are summarized in Table 3.

https://doi.org/10.5194/hess-2021-426
Preprint. Discussion started: 8 September 2021

Hydrology and Earth System Sciences
Discussions

$\mathbf{n_z}$	$\mathbf{b}$	$\mathbf{\Delta z}$ [cm]
200	0	0.01, ..., 0.01
110	$1.01 \cdot 10^{-2}$	1.00, 1.01, ... , 2.96, 2.99
49	$4.66 \cdot 10^{-2}$	1.00, 1.05, ... , 10.0, 10.5
32	$9.71 \cdot 10^{-2}$	1.00, 1.10, ... , 17.3, 19.0
18	$2.40 \cdot 10^{-1}$	1.00, 1.24, ... , 32.0, 39.8
11	$5.28 \cdot 10^{-1}$	1.00, 1.53, ... , 45.7, 69.9
8	$9.19 \cdot 10^{-1}$	1.00, 1.92, ... , 50.2, 96.4

Table 3. Grid layouts for the experiments with geometric grids. n_z is the number of vertical layers, b is the stretch factor and Δz indicates the range of layer thickness.

3.2 Experiment A: Convergence Analysis in an Idealized Infiltration Setup

In the first experiment, the soil column is forced with a constant precipitation rate of $P = 20\,\mathrm{mm\,h^{-1}}$. This rate exceeds the saturated hydraulic conductivity for both the MVG and the RT soil hydraulic model. Thus, the upper soil saturates quickly, surface runoff sets in, and a sharp wetting front forms subsequently in the soil. Table 2 gives an overview on the model setups tested. The precipitation forcing is kept up until the soil column is fully saturated for all tested setups and then run with the same forcing up to a total of 33.6 hours. The forcing is then stopped and the simulations are subject to a drainage processes steered entirely by groundwater runoff (see section 2.2.3) for the same amount of time, leading to a total model runtime of 67.2 hours. Experiment **A** run on a regular grid is denoted **AR**, while on a geometric grid it is marked **AG**.

This experiment has two different purposes: The first one is to test whether the model can accurately reproduce the analytical solution for a fully saturated soil column. This allows for checking whether the model is running correctly. The second purpose is to check, whether the numerical approximation of the infiltration process converges, that is to test whether the propagation of the wetting front depends on the choice of the numerical grid and the time step. If the solution converges, it is possible to define a range of acceptable choices for grid setup and time step respectively.

The simulation with 200 equidistant soil layers of $\Delta z = 1$ cm thickness and with a temporal resolution of $\Delta t = 1\,\mathrm{s}$ is defined as the reference simulation and numerical convergence is always investigated with respect to this reference. As a metric of convergence, normalized root mean squared differences of surface runoff Q_S with respect to the reference simulation are calculated by

$$NRMSD = \frac{\sqrt{\frac{1}{n_t}\sum_{i=1}^{n_t}\left(Q_{S,i} - Q_{S,i}^{(ref)}\right)^2}}{\frac{1}{n_t}\sum_{i=1}^{n_t} Q_{S,i}^{(ref)}}\,, \tag{18}$$

https://doi.org/10.5194/hess-2021-426
Preprint. Discussion started: 8 September 2021


Hydrology and Earth System Sciences
Discussions

where i denotes the time step and n_t the number of time steps in the simulation under investigation. In order for the number of time steps of the reference simulation to match, surface runoff in the reference run is averaged to the time levels of the simulation under investigation.

3.3 Experiment B: Convergence Under Realistic Precipitation Forcing

As experiment **A** is subject to a rather unrealistic forcing, a second experiment with a more realistic precipitation forcing is required to assess the dependence of the infiltration-runoff partitioning on the numerical setup of our model. To this end, time series are extracted from two COSMO v5.0 simulations carried out following Zeman et al. (2021) over the European domain from May 29 00:00 UTC to May 31 00:00 UTC 2018. These 48 h are characterized by strong convective activity across Central and Northern Europe. The simulations have a horizontal resolution of $0.1°$ (12 km) and $0.02°$ (2.2 km) and corresponding time steps of 90 s and 20 s, respectively. For the experiment presented here, precipitation forcing needs to be available for individual time steps, and therefore the simulations were re-run with a high output frequency and otherwise identical setup as presented by Zeman et al. (2021). Deep convection is parameterized with the Tiedtke (1989) convection scheme for the 12 km simulation and explicitly considered in the 2.2 km simulation. The shallow convection parameterization scheme (Tiedtke, 1989) is switched on for both simulations. Fig. 1 shows the 24 h sum of precipitation as obtained from the two simulations. One local maximum which is present in both simulations is located at the Southern Alpine Ridge at slightly different, yet very close locations near the village of Baceno and the mountain peak Pizzo Tambo. Time series are extracted from the single closest grid points to Baceno (for the 2.2 km simulation) and Pizzo Tambo (for the 12 km simulation) respectively (red points in Fig. 1). To disentangle impacts of the convection parameterization from impacts of spatial averaging, another time series is derived by remapping the 2.2 km simulation conservatively to the 12 km grid and then again extracting the grid point closest to Baceno. Furthermore, the extracted time series are also aggregated to different time levels in order to differentiate time step dependence in our model from smoothing effects in the precipitation forcing time series. Table 4 summarizes all time series carried out within the framework of experiment **B** and an overview on model setups for experiment **B** is given in Table 2. As in Experiment

ID	Location	Native Δx	Agg. Δx	Native Δt	Agg. Δt
B1	Baceno	2.2 km	-	20s	-
B2	Baceno	2.2 km	-	20s	90s
B3	Baceno	2.2 km	12 km	20s	-
B4	Baceno	2.2 km	12 km	20s	90s
T1	P. Tambo	12 km	-	90s	-

Table 4. Summary of time series extracted from two simulations carried out after Zeman et al. (2021). Native and Agg. mean the scale (both temporal and spatial) of the original and the aggregated timeseries respectively.

A, numerical convergence is measured with respect to a high-resolution reference simulation ($\Delta z = 1\,\mathrm{cm},\ \Delta t = 1\mathrm{s},\ n_z = 200$)

https://doi.org/10.5194/hess-2021-426
Preprint. Discussion started: 8 September 2021


Hydrology and Earth System Sciences
Discussions

4 Results

4.1 Comparison to the Analytical Solution of the Fully Saturated Steady-State in Experiment A

Before the results from the numerical experiments are presented, an analytical solution to the Richards equation is presented for a special case. We consider the case of a fully saturated soil where the volumetric soil moisture corresponds to the total pore volume ($\theta = \eta$). Furthermore let us assume stationarity ($\partial\theta/\partial t = 0$), by assuming that the water loss due to ground runoff is always balanced by infiltration from above. Under these assumptions, (4) reduces to

$$\frac{\partial K}{\partial z} = -Q. \tag{19}$$

Given the boundary condition at the bottom $K\left(z = z_b\right) = 0$, it is straightforward to find the analytical solution for (19). As there is no explicit dependence of K on z, (19) can be solved by separation of variables ($\forall z \in [0, z_b]$) and the solution formally reads,

$$K\left(z\right) = \int_{z}^{z_b} Q(z)\mathrm{d}z \ . \tag{20}$$

Plugging this into the Schlemmer et al. (2018) formulation for ground runoff given by (5), the integral is straightforward to evaluate and yields

$$K\left(z\right) = L_g^{-1} \cdot S_{\mathrm{ORO}} \cdot K_0 \cdot \left(z_b - z\right) \ . \tag{21}$$

As Q is given by the Schlemmer et al. (2018) model and K by the soil hydraulic model, the equation is inconsistent, except if the free parameter L_g^{-1} is chosen in an appropriate way which may easily be derived from (19). If one chooses a free drainage boundary condition, the consistency of (19) is naturally given (but only in the absence of a sink, such as e.g. evapotranspiration). In the case of the (Schlemmer et al., 2018) runoff, it is likely that the flux corrections adjust K to match (21), this is however not included in their analytical setup of the model. The inconsistency arises, because the saturation form of Richards equation is (strictly speaking) not applicable for fully saturated soils (A). Nevertheless, if K is allowed to adjust, ground runoff Q dictates the steady-state solution for K. This is of course simply a consequence of mass conservation – what drips out at the bottom must be refilled at the top in order to sustain the equilibrium. Such a steady-state solution can only be reproduced with a numerical solver, if the chosen scheme is mass-conserving. For any implementation based on flux corrections (here, in particular Schlemmer et al., 2018), (21) implies that the infiltration should be part of the flux correction, because otherwise there will be a discontinuity in K at $z = 0$.

There is another important consequence of (19): If the solution of K at the surface exceeds K_0, the equilibrium solution given by (21) cannot be sustained. Such a solution can only exist, if $K(z = 0) \leq K_0$, which implies that we can find a maximum soil depth $z_{b,max}$ for which a stationary solution with a saturated soil is possible,

$$z_{b,max} < \frac{1}{L_g^{-1} \cdot S_{\mathrm{ORO}}} \ . \tag{22}$$

https://doi.org/10.5194/hess-2021-426
Preprint. Discussion started: 8 September 2021

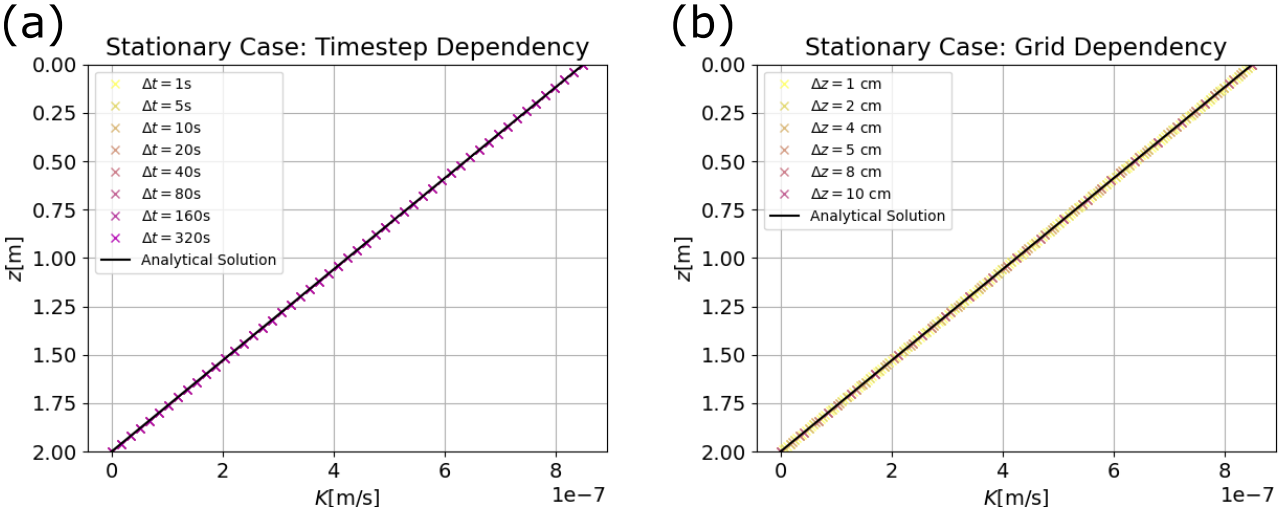

Figure 4. Hydraulic conductivity at the fully saturated steady-state in **AR**. Numerical solutions for different setups are shown for the individual levels with markers ('x'), the analytical solution is shown as solid black line. **(a)**: Solutions for Δz=4 cm with varying time steps. **(b)**: Solutions for for $\Delta t = 1$s with varying grid spacings.

Or – looking at it the other way round – this equation also determines the highest possible position of the water table for a given combination of L_g^{-1} and S_{ORO}. As an example, let $L_g^{-1} = 0.4\,\mathrm{m}^{-1}$, which is the default value for the Schlemmer et al. (2018) model and $S_{\mathrm{ORO}} = 0.2$ which corresponds to a grid point e.g. in a mountainous environment. In this example, we find $z_b < 12.5$ m.

The black line in Fig. 4 shows the analytical solution for hydraulic conductivity K for the fully saturated steady-state case. A time slice at $t = 22$ h is then extracted from all simulations in experiment **AR** (Experiment **A**, regular grids). The numerical solutions found for the different setups reproduce the analytical solution accurately and a selection is shown in Fig. 4. Evidently, the fully saturated steady-state is not of much practical relevance, but the good numerical convergence indicates that the scheme presented in Schlemmer et al. (2018) is indeed mass-conserving irrespective of the chosen grid.

4.2 Convergence in Infiltration Experiment A

The convergence during the infiltration process is more relevant for water partitioning at the surface and will therefore be investigated in more detail in this section. Fig. 5 (a) - (c) show time slices of saturation θ_f after 1.5, 3 and 5 h from the reference run ($\Delta t = 1\mathrm{s},\ \Delta z = 1$ cm). For all time slices, there is a sharp drop of saturation from $\theta_f = \eta$ to $\theta_f = 0.8\eta$, which marks the position of the wetting front. While the position of the wetting front changes with time, its shape remains more or less constant over time, in particular the sharp gradient of saturation is preserved and the propagation velocity is roughly uniform. Apart from the infiltration process that may be seen through the propagation of the wetting from panel (a) to panel (c), there is also an accumulation of water at the bottom of the soil column, which is due to the ground runoff formulation which

https://doi.org/10.5194/hess-2021-426
Preprint. Discussion started: 8 September 2021

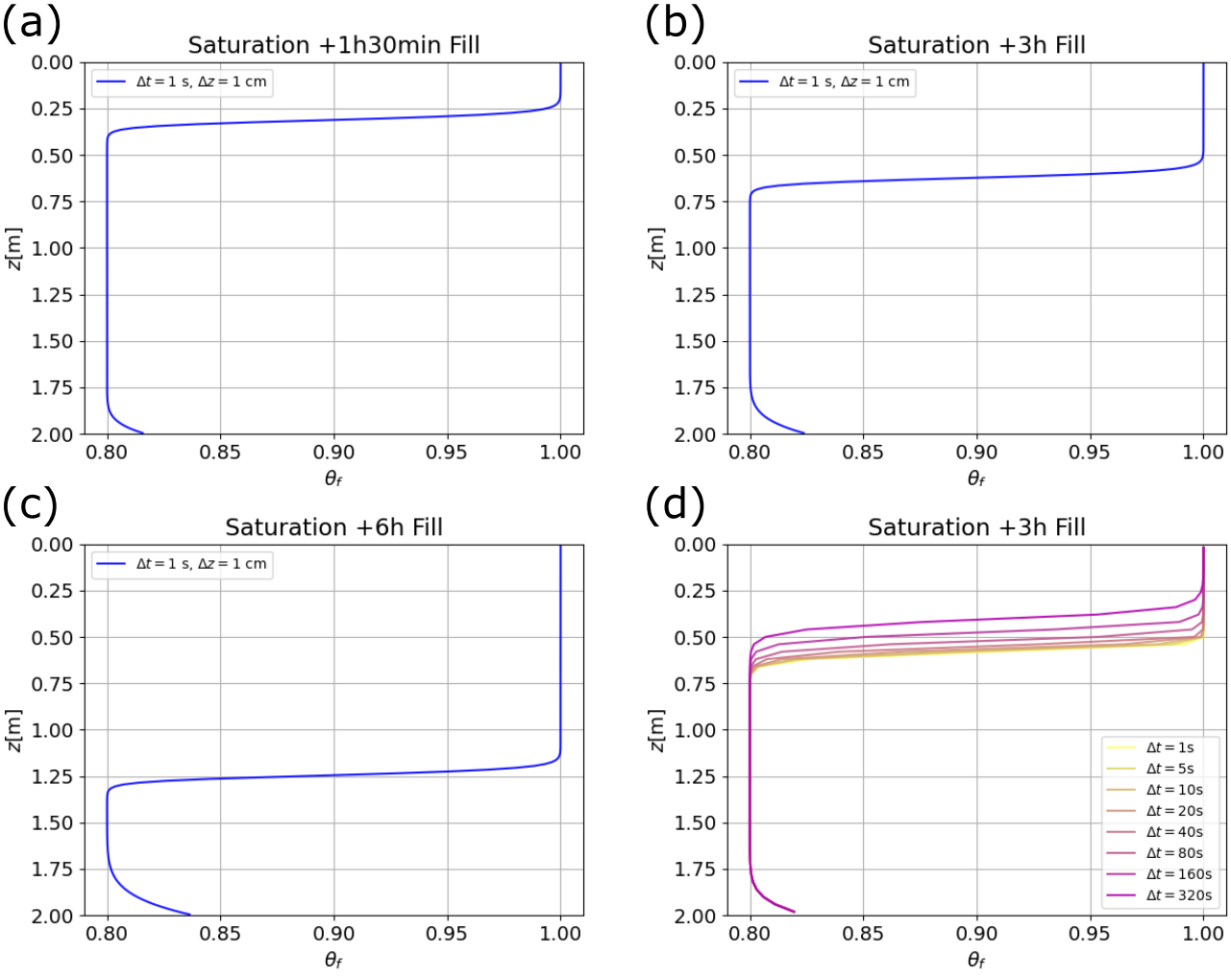

Figure 5. (a) - (c): Saturation for $\Delta t = 1$ s, $\Delta z = 1$ cm after 1.5, 3 and 6 h of forcing with a precipitation rate of $P = 20$ mm h^{-1}. **(d)**: Solutions after 3 hours of forcing for the same experiment with $\Delta z = 4$ cm and different time steps (colors).

https://doi.org/10.5194/hess-2021-426
Preprint. Discussion started: 8 September 2021

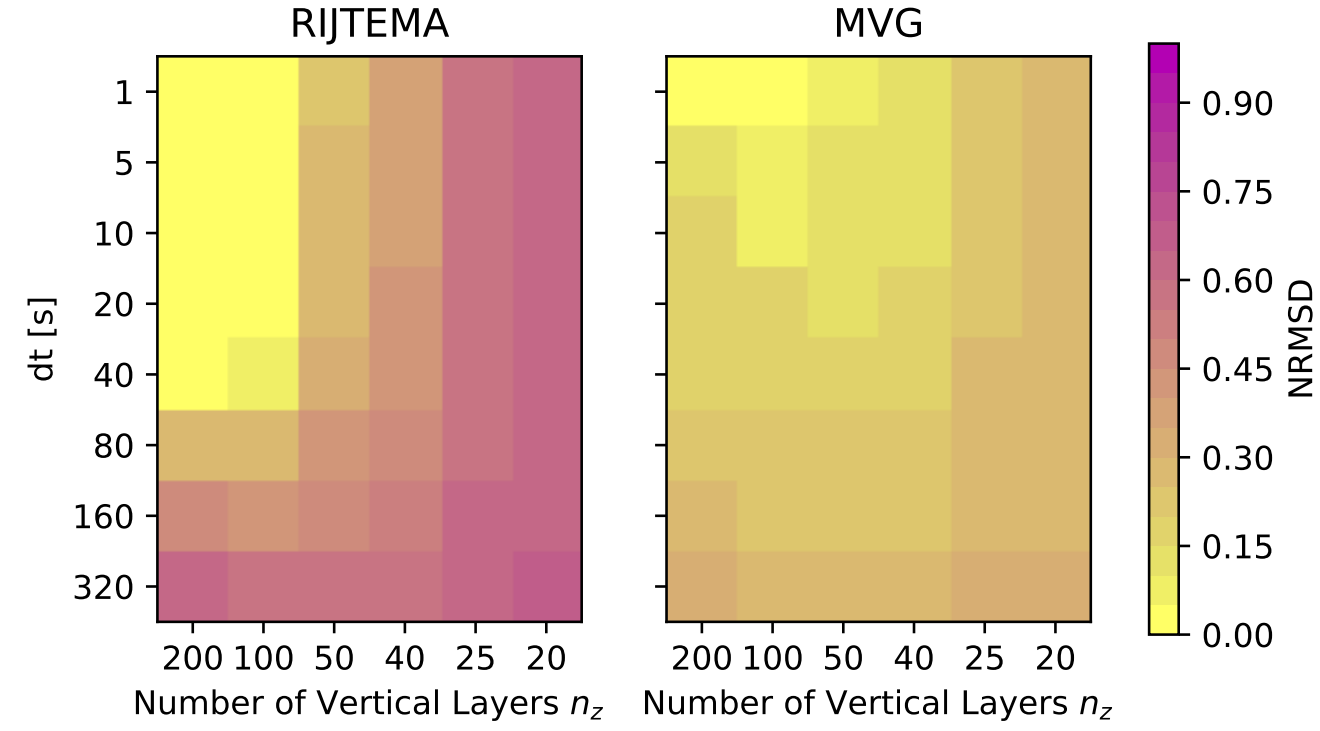

Figure 6. NRMSD of surface runoff with respect to the reference run ($\Delta t = 1\,\mathrm{s}$, $\Delta z = 0.01\,\mathrm{m}$) as a function of Δt and Δz for the RT and MVG soil hydraulic models in **AR**.

needs some time for the water table to build up before water can be transported away as ground runoff (see section 2.2.3). Fig. 5 (d) shows the same time slice as in panel (b) but for different time steps. The solution converges as is apparent from the comparison of panels (b) and (d) and for time steps shorter or equal to 40 s, differences are barely visible by eye. For time steps longer than 40 s, the deviation from the solution seems to be relevant and systematic as a pronounced slowdown of the wetting front is observed with increasing time step.

4.2.1 Equidistant Grid, AR

The systematic slowdown of the wetting front with increasing time step calls for a more systematic analysis which is presented in Fig. 6, where NRMSD values in surface runoff with respect to the reference run are shown for all model setups described in experiment **AR**. There are marked differences in convergence for the MVG and the RT soil hydraulic models. For both parameterizations, the NRMSD is smaller than 20 % if $\Delta t \leq 40\,\mathrm{s}$. For the RT parameterization, only setups with $\Delta z \leq 2\,\mathrm{cm}$ have NRMSD values smaller than 20 % and the NRMSD then increases fast with decreasing vertical resolution. The same is true for time steps longer than 40 s. In general, the NRMSD is smaller for the MVG parameterization except for a rather small range of time steps smaller than 40 s and vertical resolutions of 1 cm and 2 cm, where simulations with the RT parameterization

https://doi.org/10.5194/hess-2021-426
Preprint. Discussion started: 8 September 2021

Hydrology and Earth System Sciences
Discussions

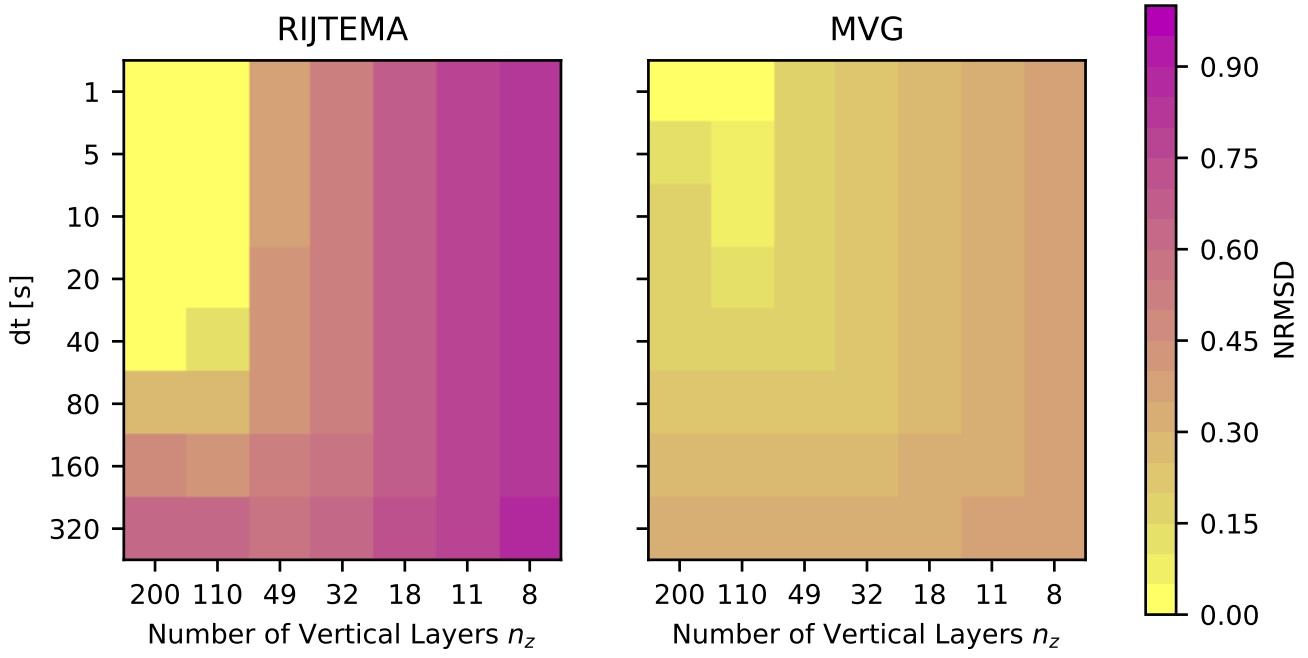

Figure 7. NRMSD of surface runoff with respect to the reference run ($\Delta t = 1\,\mathrm{s}$, $\Delta z = 0.01\,\mathrm{m}$) as a function of Δt and stretch factor b for the RT and MVG soil hydraulic models in **AG**. Irrespective of the stretch factor b, the uppermost layer thickness is chosen to be $\Delta z_1 = 0.01\,\mathrm{m}$ and the total depth is $z_b = 2\,\mathrm{m}$.

converge better. Still, the NRMSD values are around 30 % for most model setups with the MVG parameterization, which is considerable. One important reason for the better convergence of the MVG parameterization is that the diffusion close to saturation is much higher than in the RT parameterization. This weakens the sharp gradient around the wetting front and it is therefore easier to resolve it with coarser resolution setups. An experiment with the hydraulic diffusion at saturation $D_{MVG}(\theta = \eta)$ limited to that of the RT parameterization exhibits NRMSD values that are comparable in magnitude to those found for the RT parameterization (B).

4.2.2 Geometric Grid, AG

Fig. 7 shows NRMSD values for the geometric grid setups. As is the case for regular grids, simulations with the MVG parameterization tend to converge better. Reasonable convergence in the sense that the NRMSD does not exceed 20 % is only achieved for the simulations with $b = 0, n_z = 200$ (which corresponds to the regular 1 cm grid) and for $b = 1.01 \cdot 10^{-2}, n_z = 110$ and again only for time steps less or equal to 40 s.

https://doi.org/10.5194/hess-2021-426
Preprint. Discussion started: 8 September 2021


Hydrology and Earth System Sciences
Discussions

4.2.3 A Closer Look at the Wetting Front

The relatively high NRMSD for long time steps and low resolution grids in Figs. 6 and 7 raises the question whether one can identify an underlying reason for the rather poor numerical convergence. It is illustrative to reconsider Fig. 2 and to again appreciate the sharp gradient between dry and wet zones in the sand. The formation of such gradients is an inherent characteristic of the dynamics described by Richards equation and it is critical to resolve them as well as possible. The propagation of the wetting front is not solely driven by the gravitational part of the flux K, the diffusive flux D plays an equally important role as shall be explained in the following. The contribution of the two fluxes to the moistening of the soil is shown in Fig. 8 in terms of tendencies, which are given by

$$\begin{aligned} \left(\frac{\partial\theta}{\partial t}\right)_K &= -\frac{\partial K}{\partial z} \\ \left(\frac{\partial\theta}{\partial t}\right)_D &= \frac{\partial}{\partial z}\left(D(\theta)\frac{\partial D}{\partial z}\right) . \end{aligned} \tag{23}$$

First, consider the tendencies for the reference run (top row). As is the case for the saturation gradient, the shape (but not the vertical location) of the tendencies is very similar after 1.5 hours and after 6 hours. The diffusive flux acts downstream of the conductive flux, effectively smearing out the saturation gradient slightly. While the contribution of the diffusive flux to the total tendency is smaller than the contribution of the conductive flux, it plays a major role in 'pre-wetting' the soil matrix in front of the tendency maximum. This increase in saturation θ_f in advance of the wetting front subsequently enhances K, which is very sensitive to θ_f in both (MVG and RT) soil hydraulic models. The anatomy of the wetting front is important in order to understand, why coarse resolution setups do not only fail to capture the sharpness of it but subsequently also fail to reproduce the correct propagation velocity. The thicker the layers underneath the wetting front are, the slower θ_f increases. This is illustrated by the broader saturation gradient in a coarse resolution setup ($\Delta z = 10$ cm) (Fig. 8, bottom row, blue line). As there is a strong, nonlinear dependency of D and K on θ_f, slower moistening of a layer leads to a delayed acceleration of the fluxes and subsequently to a slowdown of the wetting front with respect to the high resolution setup. This becomes very clear when considering setups with geometric grids as shown in the middle row of Fig. 8. After 1.5 hours, the position and shape of the wetting front is comparable to the wetting front of the reference run, because the layer thicknesses are similar in the uppermost part of the soil. After 6 hours, the shape of the wetting front looks more similar to the one found in the low resolution setup and the position of the wetting front is delayed with respect to the reference run, but not as much as is the case for the coarse resolution setup – indicating a decrease in propagation velocity with increasing layer thickness. The consequence on water partitioning is immediately clear from the position of the wetting front after 6 hours: It is located more than 25 % further up in the low resolution simulation, which of course translates directly to more than 25 % less water in the soil at that moment and it will become more, the longer the infiltration process lasts. While the situation looks better for the telescope setup, it is evident from the considerations in this section that the convergence will worsen over time.

https://doi.org/10.5194/hess-2021-426
Preprint. Discussion started: 8 September 2021

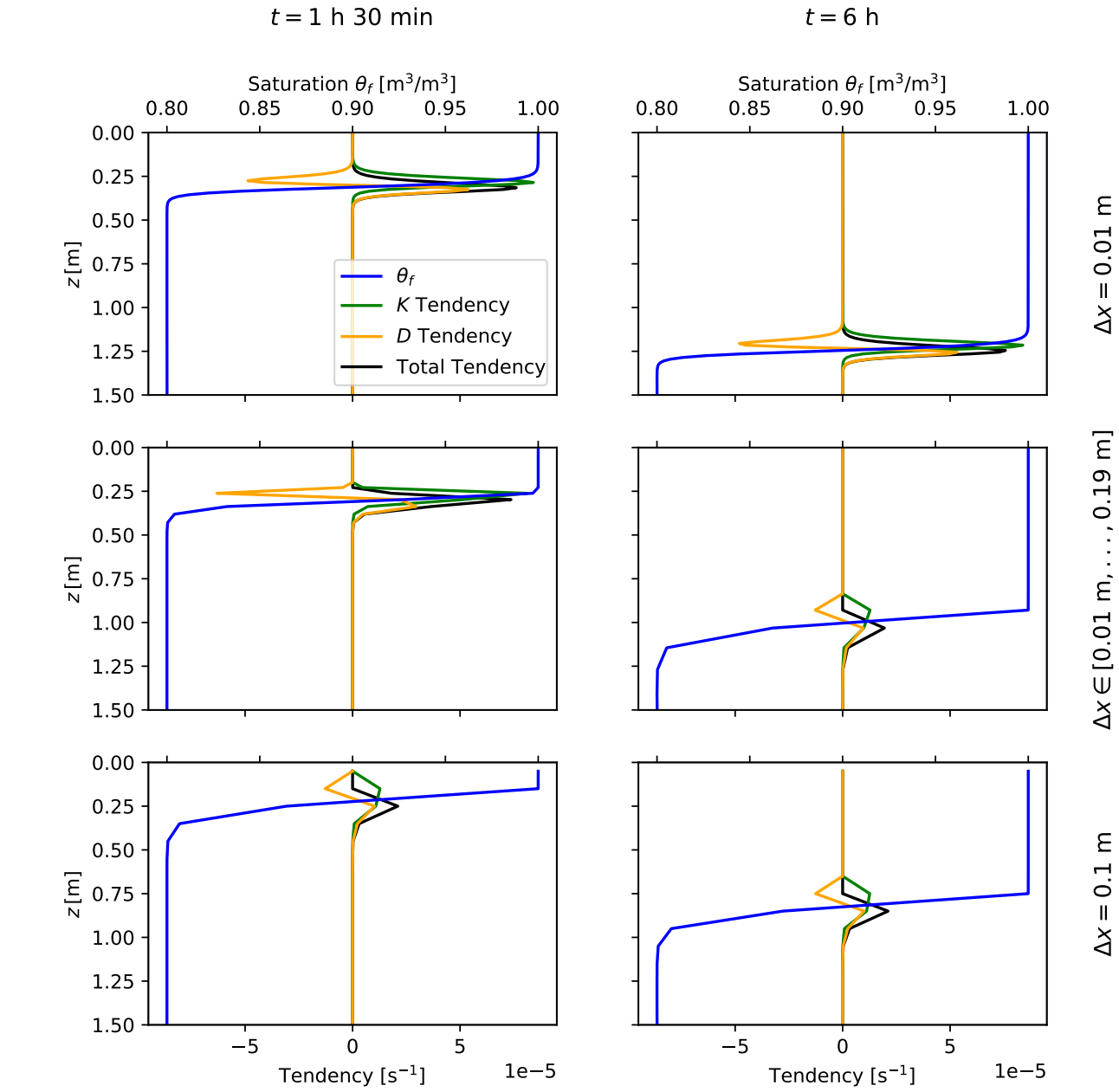

Figure 8. Contributions of conductive fluxes (green lines) and diffusive fluxes (orange lines) to soil water tendencies (black lines) during infiltration at $t = 1$ h 30min and $t = 6$ h for (a), (b) equidistant spacing of $\Delta z = 0.01$ m, (c), (d) equidistant spacing of $\Delta z = 0.1$ m and (e), (f) geometric grid with 32 vertical layers ranging from $\Delta z_1 = 0.01$ m to $\Delta z_{32} = 0.19$ m. The time step is $\Delta t = 1$ s for all simulations.

https://doi.org/10.5194/hess-2021-426
Preprint. Discussion started: 8 September 2021

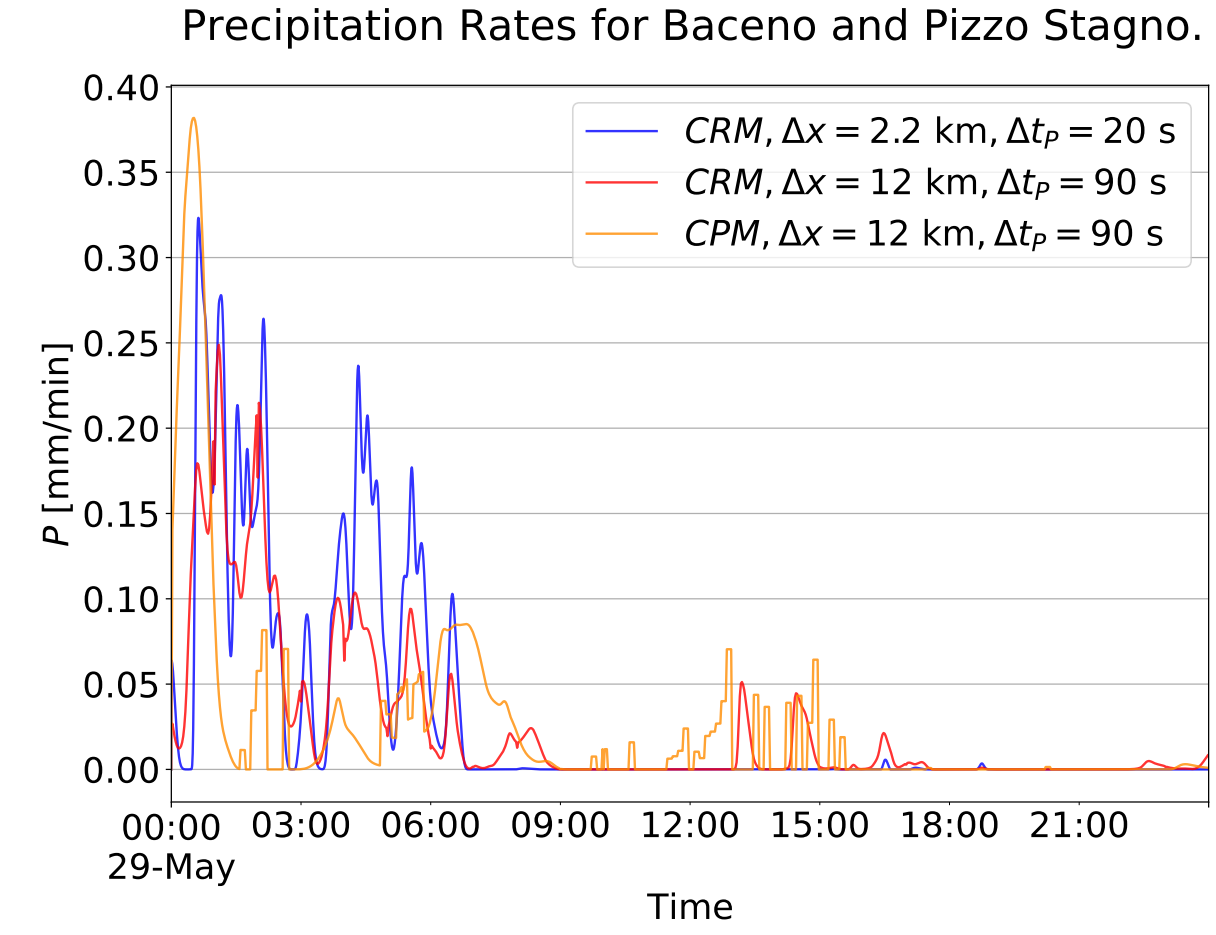

Figure 9. Precipitation time series as extracted from three different simulations after Zeman et al. (2021) (B1, B3 and T1 from Table 4). The time series are extracted from individual grid points of the 2.2 km simulation (blue), the 12 km simulation (orange), and the 2.2 km aggregated to the 12 km grid (red). The location of the grid points is indicated in Fig. 1

.

4.3 Convergence in Infiltration Experiment B

The rather poor convergence in experiment **A** is of some concern, but due to the constant high intensity precipitation forcing, the implications might be less severe in a more realistic setup. Time series are extracted from the CRM and CPM simulations described in section 3.3. An overview can be found in Table 4 and a selection of three time series (B1, B3 and T1) is shown in Fig. 9. The highest intensity precipitation peak is found in the CPM simulation shortly after 00 UTC on May 29, but subsequently the CRM simulation exhibits higher precipitation intensities. The intensities in the CRM simulation aggregated to the 12 km grid are lower than the intensities found for the native grid but the temporal evolution is very similar. This

https://doi.org/10.5194/hess-2021-426
Preprint. Discussion started: 8 September 2021

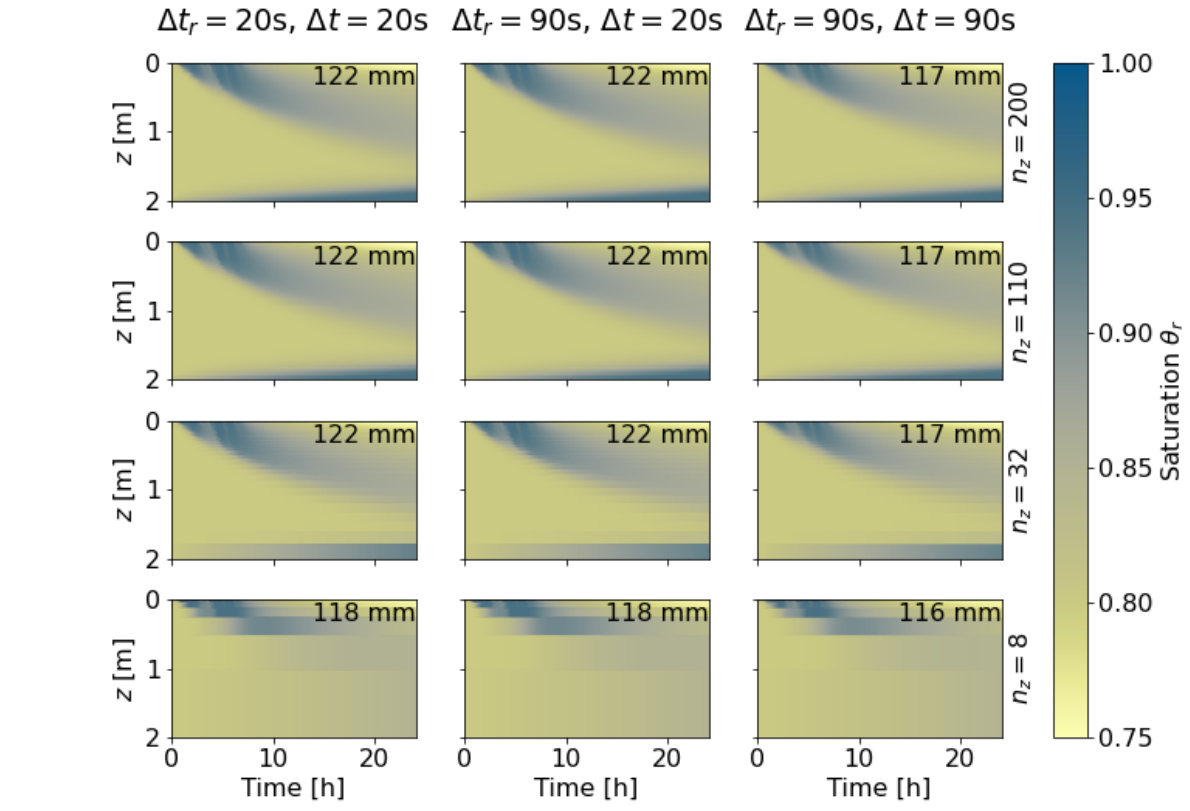

Figure 10. Saturation as a response to the forcing from the precipitation time series B1 and B2 (Tab. 4). Rows are grouped by vertical resolution. Columns are grouped by input time step Δt_r and model time steps Δt. The total amount of infiltrated water is given in the top right corner of each panel.

is an expected effect of the spatial averaging. An interesting sidenote concerns the well-known 'flickering' of the convection scheme (see e.g. Guichard et al., 2004) which is visible in the time series of the CPM simulations between 9:00 and 15:00 UTC.

The infiltration process as a response to the timeseries from the convection resolved model for different soil model setups is shown in Fig. 10. For simplicity, the analysis of experiment **B** will be focused on just four different grid setups with ($n_z = 200, 110, 32, 8$). At first glance, the process seems to be captured in a similar way by all simulations except for the low resolution simulations with $n_z = 8$. In this case, the resolution is simply too coarse to resolve the propagation of the wetting front. For the intermediate resolution case ($n_z = 32$), the propagation of the wetting front is captured, but the accumulation of water in the deep soil is very different from the reference ($n_z = 200$) and high resolution setups ($n_z = 110$), leading to a diverging behaviour of the Schlemmer et al. (2018) model (not shown). This is beyond the scope of this paper as it is model

https://doi.org/10.5194/hess-2021-426
Preprint. Discussion started: 8 September 2021


Hydrology and Earth System Sciences
Discussions

specific and the focus is on the infiltration process which is more similar across different LSMs. At closer look, it can also be seen that the infiltration of water reaches deeper for the $\Delta t = 20\,\mathrm{s}$ than it does for the $\Delta t = 90\,\mathrm{s}$, while the effect of the input time step Δt_r seems to be negligible.

Still, the time step and grid dependency shown in Fig. 10 is somewhat inconclusive and the consequences on water partitioning are again investigated by comparing surface runoff of the individual simulations. Fig. 11 summarizes the surface runoff response of different simulations to the precipitation forcing given by the the time series in Table 4. Here, accumulated runoff is shown as it is the quantity that will eventually determine soil water availability after rainfall events. The focus is thereby on the first 16 hours as the precipitation amount seems negligible afterwards (Fig. 9). The most striking feature of Fig. 11 are the almost exactly identical surface runoff curves produced by grid setups with $n_z = 200$, $n_z = 110$ and $n_z = 32$, which is why one can identify virtually only two different lines on all panels. The accumulated surface runoff for the low resolution case $n_z = 8$ differs significantly from simulations with other grid setups. It is very important to note that the differences in absolute amounts of water are most pronounced for short time steps and precipitation forcing from high resolution CRM simulations (top row) – the situation found in convection resolving NWP and climate models, where grid setups with eight layers covering roughly two meters of soil (or less) are common (e.g. Heise et al., 2003; Balsamo et al., 2009; Niu et al., 2011; Ducharne, 2016; Reick et al., 2021). The differences between low and high resolution setups are still considerable for simulations with forcing time series from the aggregated CRM (B3 and B4, middle row), but small for simulations with forcing from CPM models (T1, bottom row). As is the case in Fig. 10, the temporal aggregation of rainfall to $\Delta t_s = 90\,s$ has a negligible effect on the simulation's response (first two panels of the top and the middle row). In stark contrast, if the model time step is raised to 90 s, the differences are clearly visible and the effect is most pronounced for the $2.2\,\mathrm{km}$ precipitation forcing (compare top row, 2nd and 3rd panel). The systematic increase of surface runoff with increasing time step is evident for all considered forcing time series. Interestingly, the importance of the vertical resolution seems to decrease with increasing time step, indicating that the time step is the dominant factor for convergence.

Under CRM forcing, low resolution simulations with $\Delta t = 180\,\mathrm{s}$ and $n_z = 8$ produce more than twice the amount of surface runoff than high resolution simulations with $\Delta t = 20\ \mathrm{s}, n_z = 200$. If only the effects of vertical resolutions are considered, the differences still amount to more than 50 % of the surface runoff formed in the high resolution simulation. These are considerable amounts of water which are 'lost' in low resolution setups, simply due to the poor numerical convergence.

5 Conclusions

In this work, we investigated the sensitivity of a common numerical implementation of the Richards Equation with respect to spatial and temporal resolution, and addressed the implications on infiltration and surface runoff processes in land-surface models. In particular, we assessed the effects of the precipitation intensity, time step and vertical discretization on the hydrological part of a LSM, to frame the implications for the rainfall-runoff partitioning for kilometer-scale modeling. To this end a simple model of the one-dimensional Richards equation was developed following the equations presented by Schlemmer et al.

https://doi.org/10.5194/hess-2021-426
Preprint. Discussion started: 8 September 2021

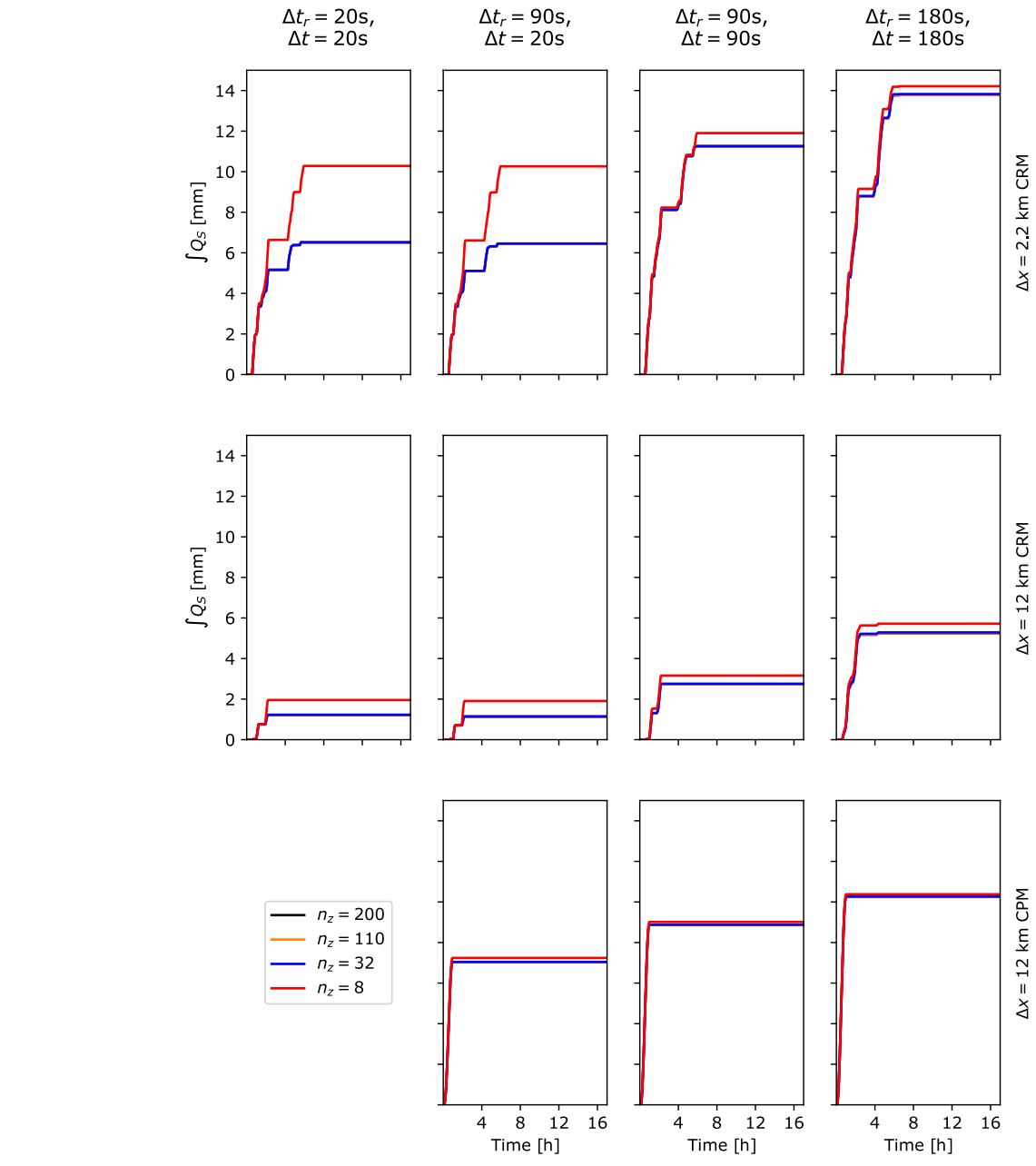

Figure 11. Accumulated surface runoff in response to the forcing from the precipitation time series listed in Table 4. The panels are grouped by forcing time series and model time step. The rows are grouped by the different simulations from which the forcing time series are extracted (2.2 km CRM, 12 km CRM and 12 km CPM respectively. The columns are grouped by forcing time step Δt_r and model time step Δt. Different colors stand for different vertical resolutions.

https://doi.org/10.5194/hess-2021-426
Preprint. Discussion started: 8 September 2021


Hydrology and Earth System Sciences
Discussions

(2018). The vertical discretization was improved by introducing a coordinate transform which allows for a 2nd-order accurate representation of the solution. The model was then applied to investigate the infiltration process. In a first experiment, the model was exposed to constant precipitation rates of 20 mm per hour to investigate the convergence of the infiltration process. We then carried out a second experiment with precipitation time series obtained from convection resolving and convection parameterized simulations to asses the impact of numerical convergence on water partitioning at the surface. The main findings of these experiments are:

- Poor convergence for regular grids with a vertical resolution coarser than $4\ \mathrm{cm}$.
- Poor convergence for time steps longer than 40 s.
- Better convergence for the Mualem - van Genuchten model than for the Rijtema model.
- Similar situation for unequally-spaced geometric grids, poor convergence for grids with 49 or less vertical layers on a total depth of 2 m.
- Systematic decrease of the propagation velocity of the wetting front with decreasing vertical resolution and increasing time step.
- When forced with realistic precipitation time series, the amount of generated surface runoff is more than 50 % higher for low resolution setups than for high resolution setups.
- If long time steps are chosen, the situation is even worse with low resolution setups generating up to 100 % more surface runoff than their high-resolution counterparts.

It is assumed that the strong gradients around the wetting front must be resolved in order to capture the propagation of the wetting front accurately. If the vertical resolution or the time stepping fail to resolve the propagating wetting front, the poor convergence of the infiltration process translates directly to a poor convergence of water partitioning at the surface.

Seven or eight layers covering a two meter soil column is not uncommon in many state of the art LSMs. At these resolutions it might be not appropriate to think of the scheme as an approximation to Richards equation. Instead one may think of it as moving water between boxes of fixed size. This is important as in the latter case, the choice of box size matters a lot for the dynamics of the system and this should be made transparent for model developers and users alike to avoid unwanted effects when the layering is changed.

The detailed analysis illustrates that there are compensating effects at play: while rainfall intensities increase in CRMs, favoring more surface runoff, the employed time step decreases, enabling a better numerical representation of the infiltration process and thus reducing unrealistic runoff.

In the full comparison between CPM and CRM simulations, other factors like differing soil types and interception reservoir sizes interfere with the uncertainties arising due to inaccurate numerical approximations of the Richards equation. If the aim is – and it must be – to have similar representations of the terrestrial water cycle across horizontal resolutions, model tuning is

https://doi.org/10.5194/hess-2021-426
Preprint. Discussion started: 8 September 2021


Hydrology and Earth System Sciences
Discussions

a rather cumbersome endeavour in the presence of such numerical uncertainties. Yet, with kilometer-resolution global climate simulations at the horizon, a correct representation of the infiltration process is a key ingredient for their success.

There is also justified doubt whether the Richards equation is an adequate equation to describe vertical water movement on the scale of LSM grid cells, even for models with a tiling approach and even on the kilometer-scale, as it does not account for flow through cracks and macropores (Beven, 2010). Finally, we point out that approximations to the Richards equation with more robust convergence properties readily exist, most notably the Green-Ampt equation (Green and Ampt, 1911; Chen and Young, 2006) and the more recently developed soil moisture velocity equation (SMVE) (Ogden et al., 2017) and these equations should be considered for the use in LSMs.

Code availability. The model introduced in section 2 will be made available on GitHub: https://github.com/regDaniel along with a short documentation, run and analysis scripts.

Appendix A: Relation between saturation-, mixed- and head-based form of Richards Equation and Mathematical Issues of the Saturation Form

In order to appreciate the issue related to the saturation form Richards equation, we revisit its derivation from (3) to (4), where the hydraulic diffusivity is introduced as $D(\theta) = K(\theta)\partial h/\partial\theta$. It must be stressed that the introduction of D is not motivated by the physics of the system, but solely in order to bring the equation to a form for which solution methods readily existed at the time (namely the diffusion equation). In soil physics, the expression $C(\theta) = \partial\theta/\partial h$ is referred to as specific water capacity (see Hillel, 2012, p.158) and thus hydraulic diffusivity is the ratio of hydraulic conductivity to specific water capacity. Clearly, in the saturated part of the soil, specific water capacity must vanish and as $K(\theta)$ is finite, hydraulic diffusivity diverges,

$$\lim_{\theta\to\eta} C(\theta) = 0 \Rightarrow \lim_{\theta\to\eta} D(\theta) = \infty\ . \tag{A1}$$

Therefore the chain rule expansion $\partial h/\partial z = \partial h/\partial\theta \cdot \partial\theta/\partial z$ is mathematically invalid for fully saturated soils as it is an expansion with "$\infty \cdot 0$". This implies that one should not use the saturation form of Richards equation when the soil is expected to reach saturation. Formally, this is shown by Gilding (1991) who derives integrability conditions for D under which wetting fronts with finite propagation speed may form, at least one of which is not met by (A1). Therefore the saturation form is neither suitable to treat the infiltration problem, nor is its use adequate in the presence of water tables. This is also the underlying reason for the necessity of limiting hydraulic diffusivity in the MVG parameterization.

Apart from the issue with diverging hydraulic diffusivity pointed out in the beginning of this section, there is another closely related problematic aspect in the saturation form: Close to the water table, discontinuities in θ may appear and thus render θ not differentiable in space. In contrast, the suction head h is continuous and differentiable even in the transition region from vadose zone to water table (Farthing and Ogden, 2017).

Despite the issues explained in this appendix, it should be mentioned that the saturation form is used successfully in LSMs, even if its use is mathematically not fully appropriate. In general, the product $D(\theta) \cdot \partial\theta/\partial z$ converges (otherwise the mixed

https://doi.org/10.5194/hess-2021-426
Preprint. Discussion started: 8 September 2021


Hydrology and Earth System Sciences
Discussions

and head forms would not converge neither). In practice, it is more an issue of the numerical implementation, i.e. limiting D to finite values.

The alternative is to either use the mixed form (3) or a fully head based form which can be derived from (3) by using the chain rule to expand $\partial\theta/\partial t = \partial\theta/\partial h \cdot \partial h/\partial t$ and plugging in the definition of the specific water capacity to obtain

$$C(\theta)\frac{\partial h}{\partial t} = K(\theta)\left(\frac{\partial h}{\partial z} - 1\right) . \tag{A2}$$

The fully head-based form is usually favored by soil physicists. The reason is that if one accounts for the compressibility of water, the left hand side of (3) would contain an additional term in which the head is appearing. The numerical solution of the mixed form is thus more complicated as one needs to advance both θ and h in time (Tocci et al., 1997). In the absence of compressibility effects, the mixed form is however appropriate and solution methods exist in the soil physics literature (De Rooij, 2010).

Appendix B: Convergence using the MVG parameterization with lower diffusion limits

Experiment **AR** is repeated for the MVG soil hydraulic model with a single modification to D. The limit at saturation was set according to

$$\lim_{\theta\to\eta} D(\theta) = 3.57 \cdot 10^{-7}\frac{\mathrm{m}^2}{\mathrm{s}} , \tag{B1}$$

which corresponds to the value for D_0 (D at saturation) of the RT model. A comparison of NRMSD values between the regular MVG model and the diffusion limited (DIFFLIM) MVG model is shown in Fig. B1. The convergence for the diffusion limited MVG model is substantially poorer than for the original MVG model. Strong hydraulic diffusion acts against sharp gradients in soil moisture and it is hypothesized that this enhances convergence in the original MVG model.

Author contributions. E.J. and D.R. implemented the model in Python. C.S. and D.R. formulated the suggestion for the coordinate transformation. D.R., L.S. and C.S. wrote the manuscript.

Competing interests. The authors declare no competing interests.

Acknowledgements. The authors thank Christian Zeman for re-running his model setup in order to provide rain rates at time step level. We thank Jürgen Helmert at DWD for providing information on ongoing developments in the TERRA ML land surface model. This work is partially funded by the COSMO-WEW funding instrument of the Centre for Climate Systems Modelling (C2SM).

https://doi.org/10.5194/hess-2021-426
Preprint. Discussion started: 8 September 2021

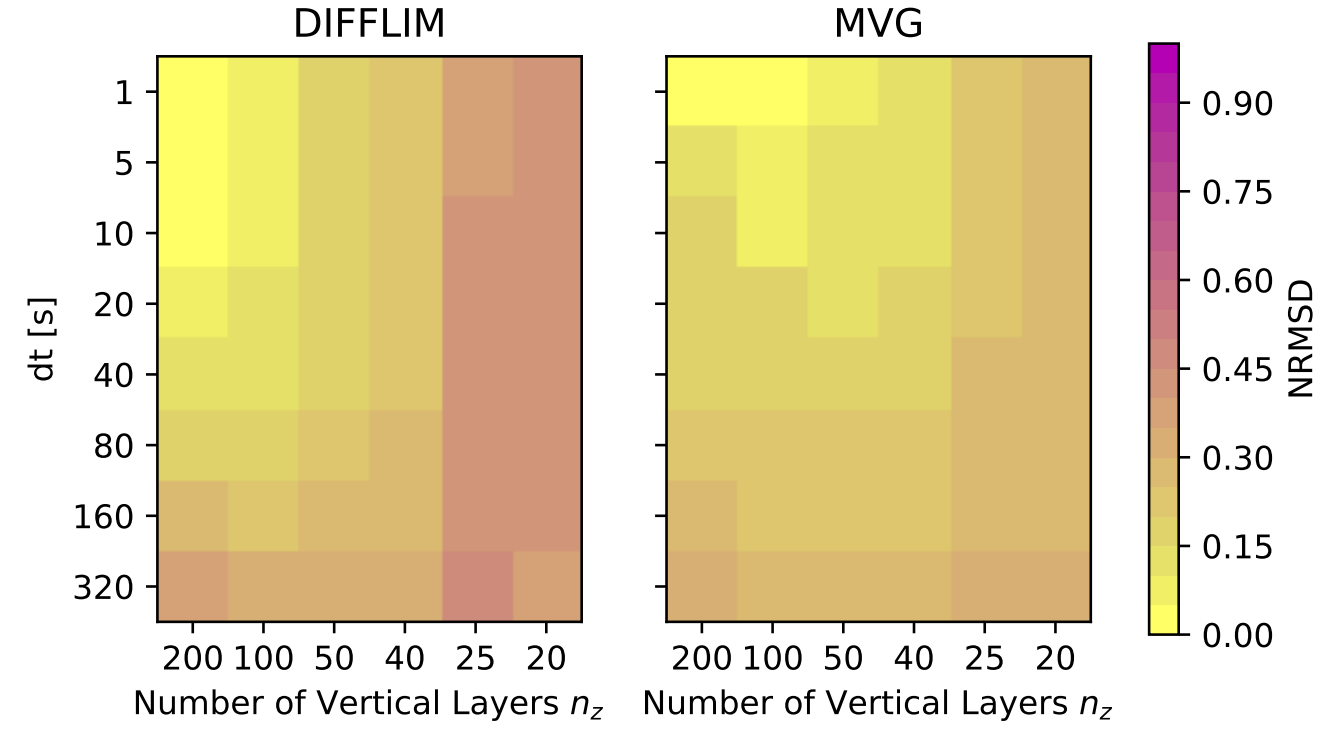

Figure B1. NRMSD of surface runoff with respect to the reference run ($\Delta t = 1\,\mathrm{s}$, $\Delta z = 0.01\,\mathrm{m}$) as a function of Δt and Δz for the DIFFLIM and MVG soil hydraulic models.

References

Baldauf, M., Seifert, A., Förstner, J., Majewski, D., Raschendorfer, M., and Reinhardt, T.: Operational convective-scale numerical weather prediction with the COSMO model: description and sensitivities, Monthly Weather Review, 139, 3887–3905, 2011.

Balsamo, G., Beljaars, A., Scipal, K., Viterbo, P., van den Hurk, B., Hirschi, M., and Betts, A. K.: A revised hydrology for the ECMWF model: Verification from field site to terrestrial water storage and impact in the Integrated Forecast System, Journal of Hydrometeorology, 10, 623–643, 2009.

Ban, N., Schmidli, J., and Schär, C.: Evaluation of the convection-resolving regional climate modeling approach in decade-long simulations, Journal of Geophysical Research: Atmospheres, 119, 7889–7907, https://doi.org/https://doi.org/10.1002/2014JD021478, 2014.

Beven, K. J.: Preferential flows and travel time distributions: defining adequate hypothesis tests for hydrological process models, Hydrological Processes, 24, 1537–1547, https://doi.org/https://doi.org/10.1002/hyp.7718, 2010.

Beven, K. J. and Cloke, H. L.: Comment on "Hyperresolution global land surface modeling: Meeting a grand challenge for monitoring Earth's terrestrial water" by Eric F. Wood et al., Water Resources Research, 48, https://doi.org/https://doi.org/10.1029/2011WR010982, 2012.

https://doi.org/10.5194/hess-2021-426
Preprint. Discussion started: 8 September 2021

Boris, J. P. and Book, D. L.: Flux-corrected transport. I. SHASTA, a fluid transport algorithm that works, Journal of computational physics, 11, 38–69, 1973.

Campoy, A., Ducharne, A., Cheruy, F., Hourdin, F., Polcher, J., and Dupont, J. C.: Response of land surface fluxes and precipitation to different soil bottom hydrological conditions in a general circulation model, Journal of Geophysical Research: Atmospheres, 118, 10,725–10,739, https://doi.org/https://doi.org/10.1002/jgrd.50627, 2013.

Chen, L. and Young, M.: Green-Ampt infiltration model for sloping surfaces, Water Resources Research, 42, https://doi.org/10.1029/2005WR004468, 2006.

Clapp, R. B. and Hornberger, G. M.: Empirical equations for some soil hydraulic properties, Water Resources Research, 14, 601–604, 1978.

De Rooij, G. H.: Comments on "Improving the numerical simulation of soil moisture–based Richards equation for land models with a deep or shallow water table", Journal of Hydrometeorology, 11, 1044–1050, 2010.

Decharme, B., Douville, H., Boone, A., Habets, F., and Noilhan, J.: Impact of an exponential profile of saturated hydraulic conductivity within the ISBA LSM: simulations over the Rhône basin, Journal of Hydrometeorology, 7, 61–80, 2006.

Ducharne, A.: The hydrol module of ORCHIDEE: Scientific documentation, 2016.

Farthing, M. W. and Ogden, F. L.: Numerical Solution of Richards' Equation: A Review of Advances and Challenges, Soil Science Society of America Journal, 81, 1257–1269, https://doi.org/https://doi.org/10.2136/sssaj2017.02.0058, 2017.

Fisher, R. A. and Koven, C. D.: Perspectives on the Future of Land Surface Models and the Challenges of Representing Complex Terrestrial Systems, Journal of Advances in Modeling Earth Systems, 12, e2018MS001 453, https://doi.org/https://doi.org/10.1029/2018MS001453, e2018MS001453 2018MS001453, 2020.

Fuhrer, O., Osuna, C., Lapillonne, X., Gysi, T., Cumming, B., Bianco, M., Arteaga, A., and Schulthess, T. C.: Towards a performance portable, architecture agnostic implementation strategy for weather and climate models, Supercomputing frontiers and innovations, 1, 45–62, 2014.

Fuhrer, O., Chadha, T., Hoefler, T., Kwasniewski, G., Lapillonne, X., Leutwyler, D., Lüthi, D., Osuna, C., Schär, C., Schulthess, T. C., et al.: Near-global climate simulation at 1 km resolution: establishing a performance baseline on 4888 GPUs with COSMO 5.0, Geoscientific Model Development, 11, 1665–1681, 2018.

Gilding, B.: Qualitative mathematical analysis of the Richards equation, Transport in Porous Media, 6, 651–666, 1991.

Green, W. H. and Ampt, G.: Studies on Soil Phyics., The Journal of Agricultural Science, 4, 1–24, 1911.

Guichard, F., Petch, J. C., Redelsperger, J.-L., Bechtold, P., Chaboureau, J.-P., Cheinet, S., Grabowski, W., Grenier, H., Jones, C. G., Köhler, M., Piriou, J.-M., Tailleux, R., and Tomasini, M.: Modelling the diurnal cycle of deep precipitating convection over land with cloud-resolving models and single-column models, Quarterly Journal of the Royal Meteorological Society, 130, 3139–3172, https://doi.org/https://doi.org/10.1256/qj.03.145, 2004.

Heise, E., Lange, M., Ritter, B., and Schrodin, R.: Improvement and validation of the multi-layer soil model, COSMO newsletter, 3, 198–203, 2003.

Hengl, T., Mendes de Jesus, J., Heuvelink, G. B., Ruiperez Gonzalez, M., Kilibarda, M., Blagotić, A., Shangguan, W., Wright, M. N., Geng, X., Bauer-Marschallinger, B., et al.: SoilGrids250m: Global gridded soil information based on machine learning, PLoS one, 12, e0169 748, 2017.

Hillel, D.: Applications of soil physics, Elsevier, 2012.

https://doi.org/10.5194/hess-2021-426
Preprint. Discussion started: 8 September 2021

Kavetski, D., Binning, P., and Sloan, S.: Adaptive time stepping and error control in a mass conservative numerical solution of the mixed form of Richards equation, Advances in Water Resources, 24, 595–605, https://doi.org/https://doi.org/10.1016/S0309-1708(00)00076-2, 2001.

Keller, M.: The diurnal cycle of Alpine summer convection in a convection-resolving model: evaluation with satellite data and sensitivity to atmospheric forcing, Ph.D. thesis, ETH Zurich, Zurich, Switzerland, https://doi.org/10.3929/ethz-a-010658332, 2016.

Lawrence, D. M., Fisher, R. A., Koven, C. D., Oleson, K. W., Swenson, S. C., Bonan, G., Collier, N., Ghimire, B., van Kampenhout, L., Kennedy, D., et al.: The Community Land Model version 5: Description of new features, benchmarking, and impact of forcing uncertainty, Journal of Advances in Modeling Earth Systems, 11, 4245–4287, 2019.

Lee, D. H. and Abriola, L. M.: Use of the Richards equation in land surface parameterizations, Journal of Geophysical Research: Atmospheres, 104, 27 519–27 526, https://doi.org/https://doi.org/10.1029/1999JD900951, 1999.

Leutwyler, D., Lüthi, D., Ban, N., Fuhrer, O., and Schär, C.: Evaluation of the convection-resolving climate modeling approach on continental scales, Journal of Geophysical Research: Atmospheres, 122, 5237–5258, 2017.

Liang, X., Lettenmaier, D. P., Wood, E. F., and Burges, S. J.: A simple hydrologically based model of land surface water and energy fluxes for general circulation models, Journal of Geophysical Research: Atmospheres, 99, 14 415–14 428, https://doi.org/https://doi.org/10.1029/94JD00483, 1994.

Mastrotheodoros, T., Pappas, C., Molnar, P., Burlando, P., Manoli, G., Parajka, J., Rigon, R., Szeles, B., Bottazzi, M., Hadjidoukas, P., et al.: More green and less blue water in the Alps during warmer summers, Nature Climate Change, 10, 155–161, 2020.

Maxwell, R. M., Condon, L. E., and Kollet, S. J.: A high-resolution simulation of groundwater and surface water over most of the continental US with the integrated hydrologic model ParFlow v3, Geoscientific Model Development, 8, 923–937, https://doi.org/10.5194/gmd-8-923-2015, 2015.

Mualem, Y.: A new model for predicting the hydraulic conductivity of unsaturated porous media, Water Resources Research, 12, 513–522, 1976.

Mueller-Quintino, A., Dutra, E., Cloke, H. L., Verhoef, A., Balsamo, G., and Pappenberger, F.: Water infiltration and redistribution in Land Surface Models, ECMWF, Technical Memorandum, 791, https://doi.org/10.21957/ppksejqu9, 2016.

Niu, G.-Y., Yang, Z.-L., Dickinson, R. E., and Gulden, L. E.: A simple TOPMODEL-based runoff parameterization (SIMTOP) for use in global climate models, Journal of Geophysical Research: Atmospheres, 110, 2005.

Niu, G.-Y., Yang, Z.-L., Dickinson, R. E., Gulden, L. E., and Su, H.: Development of a simple groundwater model for use in climate models and evaluation with Gravity Recovery and Climate Experiment data, Journal of Geophysical Research: Atmospheres, 112, https://doi.org/https://doi.org/10.1029/2006JD007522, 2007.

Niu, G.-Y., Yang, Z.-L., Mitchell, K. E., Chen, F., Ek, M. B., Barlage, M., Kumar, A., Manning, K., Niyogi, D., Rosero, E., et al.: The community Noah land surface model with multiparameterization options (Noah-MP): 1. Model description and evaluation with local-scale measurements, Journal of Geophysical Research: Atmospheres, 116, 2011.

Ogden, F. L., Allen, M. B., Lai, W., Zhu, J., Seo, M., Douglas, C. C., and Talbot, C. A.: The soil moisture velocity equation, Journal of Advances in Modeling Earth Systems, 9, 1473–1487, https://doi.org/https://doi.org/10.1002/2017MS000931, 2017.

Palmer, T.: Climate forecasting: Build high-resolution global climate models, Nature News, 515, 338, 2014.

Pichelli, E., Coppola, E., Sobolowski, S., Ban, N., Giorgi, F., Stocchi, P., Alias, A., Belušić, D., Berthou, S., Caillaud, C., et al.: The first multi-model ensemble of regional climate simulations at kilometer-scale resolution part 2: historical and future simulations of precipitation, Climate Dynamics, 56, 3581–3602, 2021.

https://doi.org/10.5194/hess-2021-426
Preprint. Discussion started: 8 September 2021

Pitman, A. J.: The evolution of, and revolution in, land surface schemes designed for climate models, International Journal of Climatology, 23, 479–510, https://doi.org/https://doi.org/10.1002/joc.893, 2003.

Prein, A. F., Langhans, W., Fosser, G., Ferrone, A., Ban, N., Goergen, K., Keller, M., Tölle, M., Gutjahr, O., Feser, F., Brisson, E., Kollet, S., Schmidli, J., van Lipzig, N. P. M., and Leung, R.: A review on regional convection-permitting climate modeling: Demonstrations, prospects, and challenges, Reviews of Geophysics, 53, 323–361, https://doi.org/https://doi.org/10.1002/2014RG000475, 2015.

Reick, C. H., Gayler, V., Goll, D., Hagemann, S., Heidkamp, M., Nabel, J. E., Raddatz, T., Roeckner, E., Schnur, R., and Wilkenskjeld, S.: JSBACH 3-The land component of the MPI Earth System Model: documentation of version 3.2, Tech. rep., MPI für Meteorologie, 2021.

Richards, L. A.: Capillary conduction of liquids through porous mediums, Physics, 1, 318–333, 1931.

Rijtema, P.: Soil moisture forecasting, Instituut voor Cultuurtechniek en Waterhuishouding, Tech. rep., Wageningen, Technical Report Nota 513, 1969.

Saxton, K. E. and Rawls, W. J.: Soil Water Characteristic Estimates by Texture and Organic Matter for Hydrologic Solutions, Soil Science Society of America Journal, 70, 1569–1578, https://doi.org/https://doi.org/10.2136/sssaj2005.0117, 2006.

Schaap, M. G., Leij, F. J., and van Genuchten, M. T.: ROSETTA: a computer program for estimating soil hydraulic parameters with hierarchical pedotransfer functions, Journal of Hydrology, 251, 163–176, https://doi.org/https://doi.org/10.1016/S0022-1694(01)00466-8, 2001.

Schär, C., Fuhrer, O., Arteaga, A., Ban, N., Charpilloz, C., Di Girolamo, S., Hentgen, L., Hoefler, T., Lapillonne, X., Leutwyler, D., et al.: Kilometer-scale climate models: Prospects and challenges, Bulletin of the American Meteorological Society, 101, E567–E587, 2020.

Schlemmer, L., Schär, C., Lüthi, D., and Strebel, L.: A groundwater and runoff formulation for weather and climate models, Journal of Advances in Modeling Earth Systems, 10, 1809–1832, 2018.

Shao, Y. and Irannejad, P.: On the choice of soil hydraulic models in land-surface schemes, Boundary-Layer Meteorology, 90, 83–115, 1999.

Stephens, G. L., L'Ecuyer, T., Forbes, R., Gettelmen, A., Golaz, J.-C., Bodas-Salcedo, A., Suzuki, K., Gabriel, P., and Haynes, J.: Dreary state of precipitation in global models, Journal of Geophysical Research: Atmospheres, 115, 2010.

Stevens, B., Satoh, M., Auger, L., Biercamp, J., Bretherton, C. S., Chen, X., Düben, P., Judt, F., Khairoutdinov, M., Klocke, D., et al.: DYAMOND: the DYnamics of the Atmospheric general circulation Modeled On Non-hydrostatic Domains, Progress in Earth and Planetary Science, 6, 1–17, 2019.

Sundqvist, H. and Veronis, G.: A simple finite-difference grid with non-constant intervals, Tellus, 22, 26–31, 1970.

Tiedtke, M.: A comprehensive mass flux scheme for cumulus parameterization in large-scale models, Monthly Weather Review, 117, 1779–1800, 1989.

Tocci, M. D., Kelley, C., and Miller, C. T.: Accurate and economical solution of the pressure-head form of Richards' equation by the method of lines, Advances in Water Resources, 20, 1–14, https://doi.org/https://doi.org/10.1016/S0309-1708(96)00008-5, 1997.

Van Genuchten, M. T.: A closed-form equation for predicting the hydraulic conductivity of unsaturated soils, Soil science society of America journal, 44, 892–898, 1980.

Van Looy, K., Bouma, J., Herbst, M., Koestel, J., Minasny, B., Mishra, U., Montzka, C., Nemes, A., Pachepsky, Y. A., Padarian, J., Schaap, M. G., Tóth, B., Verhoef, A., Vanderborght, J., van der Ploeg, M. J., Weihermüller, L., Zacharias, S., Zhang, Y., and Vereecken, H.: Pedotransfer Functions in Earth System Science: Challenges and Perspectives, Reviews of Geophysics, 55, 1199–1256, https://doi.org/https://doi.org/10.1002/2017RG000581, 2017.

Vergara-Temprado, J., Ban, N., and Schär, C.: Extreme Sub-Hourly Precipitation Intensities Scale Close to the Clausius-Clapeyron Rate Over Europe, Geophysical Research Letters, 48, e2020GL089 506, 2021.

https://doi.org/10.5194/hess-2021-426
Preprint. Discussion started: 8 September 2021


Hydrology and Earth System Sciences
Discussions

Wedi, N. P., Polichtchouk, I., Dueben, P., Anantharaj, V. G., Bauer, P., Boussetta, S., Browne, P., Deconinck, W., Gaudin, W., Hadade, I., Hatfield, S., Iffrig, O., Lopez, P., Maciel, P., Mueller, A., Saarinen, S., Sandu, I., Quintino, T., and Vitart, F.: A Baseline for Global Weather and Climate Simulations at 1 km Resolution, Journal of Advances in Modeling Earth Systems, 12, e2020MS002 192, https://doi.org/https://doi.org/10.1029/2020MS002192, e2020MS002192 10.1029/2020MS002192, 2020.

Weihermüller, L., Lehmann, P., Herbst, M., Rahmati, M., Verhoef, A., Or, D., Jacques, D., and Vereecken, H.: Choice of Pedotransfer Functions Matters when Simulating Soil Water Balance Fluxes, Journal of Advances in Modeling Earth Systems, 13, e2020MS002 404, https://doi.org/https://doi.org/10.1029/2020MS002404, e2020MS002404 2020MS002404, 2021.

Wood, E. F., Roundy, J. K., Troy, T. J., van Beek, L. P. H., Bierkens, M. F. P., Blyth, E., de Roo, A., Döll, P., Ek, M., Famiglietti, J., Gochis, D., van de Giesen, N., Houser, P., Jaffé, P. R., Kollet, S., Lehner, B., Lettenmaier, D. P., Peters-Lidard, C., Sivapalan, M., Sheffield, J., Wade, A., and Whitehead, P.: Hyperresolution global land surface modeling: Meeting a grand challenge for monitoring Earth's terrestrial water, Water Resources Research, 47, https://doi.org/https://doi.org/10.1029/2010WR010090, 2011.

Yano, J.-I., Ziemiański, M. Z., Cullen, M., Termonia, P., Onvlee, J., Bengtsson, L., Carrassi, A., Davy, R., Deluca, A., Gray, S. L., et al.: Scientific challenges of convective-scale numerical weather prediction, Bulletin of the American Meteorological Society, 99, 699–710, 2018.

Zalesak, S. T.: Fully multidimensional flux-corrected transport algorithms for fluids, Journal of computational physics, 31, 335–362, 1979.

Zeman, C., Wedi, N. P., Dueben, P. D., Ban, N., and Schär, C.: Model intercomparison of COSMO 5.0 and IFS 45r1 at kilometer-scale grid spacing, Geoscientific Model Development Discussions, 2021, 1–35, https://doi.org/10.5194/gmd-2021-31, 2021.

Zeng, X. and Decker, M.: Improving the numerical solution of soil moisture–based Richards equation for land models with a deep or shallow water table, Journal of Hydrometeorology, 10, 308–319, 2009.